J. Fluid Mech. (2020), *vol.* 884, A2. © Cambridge University Press 2019
doi:10.1017/jfm.2019.884

On the mechanism of open-loop control of thermoacoustic instability in a laminar premixed combustor

Amitesh Roy[1,†], Sirshendu Mondal[1,2], Samadhan A. Pawar[1] and R. I. Sujith[1]

[1]Department of Aerospace Engineering, Indian Institute of Technology Madras, Chennai 600 036, Tamil Nadu, India

[2]Department of Mechanical Engineering, National Institute of Technology Durgapur, Durgapur 713 209, West Bengal, India

(Received 27 August 2018; revised 27 September 2019; accepted 22 October 2019)

We identify mechanisms through which open-loop control of thermoacoustic instability is achieved in a laminar combustor and characterize them using synchronization theory. The thermoacoustic system comprises two nonlinearly coupled damped harmonic oscillators – acoustic and unsteady heat release rate (HRR) field – each possessing different eigenfrequencies. The frequency of the preferred mode of HRR oscillations is less than the third acoustic eigenfrequency where thermoacoustic instability develops. We systematically subject the limit-cycle oscillations to an external harmonic forcing at different frequencies and amplitudes. We observe that forcing at a frequency near the preferred mode of the HRR oscillator leads to a greater than 90 % decrease in the amplitude of the limit-cycle oscillations through the phenomenon of asynchronous quenching. Concurrently, there is a resonant amplification in the amplitude of HRR oscillations. Further, we show that the flame dynamics plays a key role in controlling the frequency at which quenching is observed. Most importantly, we show that forcing can cause asynchronous quenching either by imposing out-of-phase relation between pressure and HRR oscillations or by inducing period-2 dynamics in pressure oscillations while period-1 in HRR oscillations, thereby causing phase drifting between the two subsystems. In each of the two cases, acoustic driving is very low and hence thermoacoustic instability is suppressed. We show that the characteristics of forced synchronization of the pressure and HRR oscillations are significantly different. Thus, we find that the simultaneous characterization of the two subsystems is necessary to quantify completely the nonlinear response of the forced thermoacoustic system.

Key words: instability control, laminar reacting flows

1. Introduction

Lean combustion systems are prone to high-amplitude pressure oscillations that are established due to positive feedback between the acoustic pressure fluctuations (p') of the combustor and the heat release rate (HRR) fluctuations ($\dot{q}'$) taking place inside it. The occurrence of such high-amplitude self-sustained pressure oscillations

† Email address for correspondence: amiteshroy94@yahoo.in

in combustors is known as thermoacoustic instability (Lieuwen & Yang 2005). The sustainability of thermoacoustic instability depends closely on the energy balance inside the combustor. The time-averaged acoustic power production is defined as

$$\mathcal{P} = \frac{1}{NT}\int_0^{NT} p'(t)\dot{q}'(t)\,\mathrm{d}t, \tag{1.1}$$

where p' and $\dot{q}'$ are the pressure and HRR fluctuations about the mean, respectively, and N represents the total number of cycles, each having a time period of T, with which we compute the average. The necessary conditions for the growth of acoustic energy inside a combustor are given by the modified Rayleigh criterion. It states that there is a growth in acoustic energy when: (1) the instantaneous phase difference between pressure and HRR fluctuations remains bounded such that $|\Delta\phi_{p'\dot{q}'}| < \pi/2$ and (2) the volume integral of acoustic power sources in the combustor is higher than the acoustic efflux (loss) across the control surface (Rayleigh 1878; Poinsot & Veynante 2005).

The problem is exacerbated by the fact that thermoacoustic systems are exceedingly complex, and are capable of exhibiting n-periodic, quasiperiodic, chaotic and intermittent dynamics in addition to the comparatively well-studied limit-cycle oscillations (Juniper & Sujith 2018). Thermoacoustic instability is a significant problem in gas turbine engines used for propulsion and power generation systems and can lead to critical operational failures. Thus, control strategies are crucial for extending the longevity of gas turbine engines.

1.1. *Control strategies for suppressing thermoacoustic instability*

Control strategies for mitigating thermoacoustic instability are classified into passive control and active control. Active control is further referred to as active closed-loop control if there is real-time feedback from the combustor to the actuator; otherwise, it is called active open-loop control.

Passive control strategies involve design changes of the combustor to either increase the net acoustic efflux or disrupt the phase relationship of the flame–acoustic interaction, or both (Richards, Straub & Robey 2003; Noiray *et al.* 2007). Usually, acoustic damping is increased by installing baffles, dampers and resonators. In some cases, extensive design changes may be necessary, as is exemplified by the 2000 full-scale tests that the F-1 engine had to go through before the right combination of injector–baffle configuration could be finalized (Oefelein & Yang 1993). Passive control strategies are trial-and-error based, and the high cost incurred during the design and testing of passive control strategies in real-time propulsion systems proves to be a significant deterrent against this type of control strategy. However, in the absence of other viable control strategies, passive control is the most common way of dealing with thermoacoustic instability.

Active closed-loop control involves the control of thermoacoustic instability through the use of feedback mechanisms such as adaptive choker plates capable of altering upstream acoustic boundary conditions (Dowling *et al.* 1988; Dowling & Morgans 2005) or harmonic drivers to generate anti-phase sound, or anti-sound, at the frequency of thermoacoustic instability (Lang, Poinsot & Candel 1987). Such methods have shown promise but are not used extensively in the field. Reviews on the state of the art of active control of thermoacoustic instability can be found in Docquier & Candel (2002) and Zhao *et al.* (2018).

In contrast, active open-loop control is achieved through external forcing of the thermoacoustic system and does not rely on real-time feedback from the combustor. Thus, open-loop control systems are much easier to design and are considerably cheaper. In open-loop control, high-amplitude limit-cycle oscillations are controlled by subjecting them to harmonic forcing at a frequency away from the natural frequency of oscillations. Open-loop control results in a significant decrease in the amplitude of thermoacoustic oscillations through a process known as asynchronous quenching (Guan *et al.* 2019*a*; Mondal, Pawar & Sujith 2019). The term asynchronous indicates that quenching of oscillations takes place at a forcing frequency away from the frequency of limit-cycle oscillations. Although not referred to by this terminology, studies in the past (Lubarsky, Shcherbik & Zinn 2003; Bellows, Hreiz & Lieuwen 2008) have shown this state in turbulent combustors. Quenching has been hypothesized to be due to the destruction of the feedback loop responsible for thermoacoustic instability (Lubarsky *et al.* 2003), which leads to very low time-averaged acoustic power production (Guan *et al.* 2019*a*; Mondal *et al.* 2019). A number of studies have shown that quenching causes a significant decrease in the limit-cycle amplitude (greater than 80 % decrease of the root mean square (r.m.s.) value and 90 % of spectral amplitude) across a variety of combustors such as electrically heated Rijke tubes (Mondal *et al.* 2019), laminar combustors (Guan *et al.* 2019*a*) and turbulent combustors (Shcherbik *et al.* 2003; Bellows *et al.* 2008).

Despite such prospects, open-loop control, and active control in general, is constrained by the limited bandwidth of actuated fuel valves (Zhao & Morgans 2009). Besides, there is inadequate knowledge about the physical mechanisms that lead to quenching. In addition, the range of forcing frequencies over which quenching takes place is still unclear. Some studies have shown that quenching is only observed when the forcing frequency is lower than the frequency of limit-cycle oscillations (Lubarsky *et al.* 2003; Bellows *et al.* 2008; Mondal *et al.* 2019); whereas others have demonstrated that quenching is possible even if the forcing frequency is lower and higher than the frequency of limit-cycle oscillations (Balusamy *et al.* 2015; Guan *et al.* 2019*a*). However, no study has described the reason behind such a frequency dependence of asynchronous quenching in a given thermoacoustic system.

During open-loop control, the flame is perturbed simultaneously at the frequency of self-excited thermoacoustic instability and the frequency of external forcing. The presence of multiple frequencies makes it quite challenging to measure the response of the system. Nonlinear flame-describing functions, as proposed by Noiray *et al.* (2008) for measuring the nonlinear flame response at a single frequency, have been used to measure the flame response in the presence of incommensurate frequencies in the system (Orchini & Juniper 2016). However, they also pointed out the high cost of computation associated with the prediction of the amplitude of quasiperiodic oscillations. Further, Balusamy *et al.* (2017) pointed out that the determination of flame-describing functions can be quite a challenge as external forcing can trigger self-excited thermoacoustic oscillations, which can lead to unreliable approximations of the gain and phase of the flame response. Thus, alternative measurement tools are required to characterize the nonlinear flame response associated with the relatively high forcing amplitudes used for quenching of thermoacoustic oscillations.

Recent studies have attempted to quantify the nonlinear response of thermoacoustic instability to external forcing. As a result, several nonlinear phenomena such as frequency entrainment (Lieuwen & Neumeier 2002; Bellows *et al.* 2008; Balusamy *et al.* 2015), a shift in the natural acoustic response of the combustor (Lubarsky *et al.* 2003; Bellows *et al.* 2008; Balusamy *et al.* 2015) and frequency pulling/pushing

(Balusamy *et al.* 2015) have been identified. Guan *et al.* (2019*b*) showed that open-loop control through transient forcing could be used to achieve quenching of about 50 % of the amplitude of limit-cycle oscillations. In many of these recent studies, both numerical (Kashinath, Li & Juniper 2018) and experimental (Balusamy *et al.* 2015; Guan *et al.* 2019*a*,*b*; Mondal *et al.* 2019), the nonlinear interaction between forcing and thermoacoustic instability is explained using concepts of synchronization theory (Balanov *et al.* 2008). In the present work, we also resort to the framework of synchronization theory. We discuss the relevant concepts next.

1.2. *Forced synchronization*

In the framework of forced synchronization, the harmonic forcing and the self-excited limit-cycle oscillations are idealized as two oscillators which are unidirectionally coupled, i.e. only forcing affects the limit-cycle oscillations, and not vice versa. Forced synchronization is achieved whenever the frequency of the limit-cycle oscillations locks with the frequency of external forcing ($f_{n1} = f_f$), and the time evolution of the phase difference between them becomes bounded to a small interval μ ($<2\pi$) around some mean value C, i.e. $|\Delta\phi_{F,p'}(t) - C| = |\phi_F - \phi_{p'} - C| \leqslant \mu$ (Pikovsky & Maistrenko 2012). We refer to the forcing as F, the forcing frequency as f_f, the unforced natural frequency of the limit-cycle oscillations in p' as f_{n0} and the response frequency of the natural oscillations under forcing as f_{n1}, where f_{n1} may or may not be the same as f_{n0}. In the above definition, the condition of $|\Delta\phi_{F,p'}(t) - C| \leqslant \mu$ is referred to as phase locking, and the state of $f_{n1} = f_f$ is referred to as frequency entrainment of f_{n1} by the external forcing at f_f.

In general, the forced synchronization of an oscillator is characterized in terms of locking and suppression (Balanov *et al.* 2008). For small frequency detuning, $\Delta f = |f_f - f_{n1}|/f_{n0} \leqslant \epsilon$, where $\epsilon \ll 1$, the transition to synchronization is associated with the spectral peak at f_{n1} moving towards the spectral peak at f_f, when the forcing amplitude is increased. The state of synchronization achieved in this manner is called locking. For larger frequency detuning, $\Delta f = |f_f - f_{n1}|/f_{n0} > \epsilon$, upon increasing the forcing amplitude, the spectral amplitude associated with f_{n1} gradually diminishes, before vanishing completely. Synchronization attained in this manner is referred to as suppression. Thus, the states of locking and suppression are two different pathways to the same final state of forced synchronization. Each of these two pathways involves different types of bifurcations. The reader is referred to Balanov *et al.* (2008) for a general treatment of this topic and to Kashinath *et al.* (2018) and Mondal *et al.* (2019) for its implementation in thermoacoustics.

1.3. *Forced synchronization in hydrodynamic and thermoacoustic systems*

It is quite well established that thermoacoustic instability arises out of an interplay between the various subsystems inside a combustor – flow dynamics, combustion and acoustics. Thus, understanding the effect of forcing on each of these subsystems simultaneously becomes necessary. In the recent past, many studies have attempted to characterize the nonlinear effect of forcing on each of these individual subsystems and their combinations using synchronization theory.

For hydrodynamic systems, Juniper, Li & Nichols (2009) reported frequency entrainment of reacting and non-reacting, globally unstable hydrodynamic jets. For a non-reacting low-density self-excited jet, the route to forced synchronization was illustrated by Li & Juniper (2013*a*,*b*,*c*). They observed that the system response was asymmetric about f_{n0} and forced synchronization was achieved only for

$f_f < f_{n0}$. Later, Pawar *et al.* (2018) quantified the effect of forcing on a preheated bluff-body-stabilized flame. They found that synchronization characteristics of the top and bottom branch of the flame exhibit significant asymmetry depending upon the density ratio of the unburned reactants to products. These results indicate that the stability of the underlying flow field has a significant effect on its response to external forcing.

For a swirl-stabilized combustor exhibiting thermoacoustic instability, Bellows *et al.* (2008) were able to quench acoustic pressure oscillation to about 90 % of the unforced spectral amplitude and ∼65 % of the unforced r.m.s. value when $f_f < f_{n0}$. Although not discussed in their study, quenching was associated with the forced synchronization of thermoacoustic instability. In a similar system, Balusamy *et al.* (2015) observed forced synchronization of limit-cycle oscillations for both $f_f < f_{n0}$ and $f_f > f_{n0}$. However, they did not comment on the overall decrease in the amplitude of limit-cycle oscillations when forced synchronization was achieved. The locking and suppression route to forced synchronization of limit-cycle oscillation has been shown in a numerical study of a laminar burner (Kashinath *et al.* 2018) and in an experimental study of a Rijke tube (Mondal *et al.* 2019). Kashinath *et al.* (2018) also demonstrated the forced synchronization of quasiperiodic and chaotic oscillations arising in a thermoacoustic system.

Recent systematic studies of Guan *et al.* (2019*a*) and Mondal *et al.* (2019) have shed more light on asynchronous quenching. They observed that the asynchronous quenching of limit-cycle oscillation is achieved when the following conditions are satisfied: (i) limit-cycle oscillation is synchronized to the forcing and (ii) the forcing frequency is far away from the natural frequency. Asynchronous quenching has been observed in a variety of systems such as plasmas (Keen & Fletcher 1970), control systems (Fjeld 1974) and ionization waves (Ohe & Takeda 1974). However, as mentioned before, the frequency at which asynchronous quenching is observed remains a confounding aspect in recent studies of open-loop control.

1.4. *Contributions of the present study*

In many of the previous studies of open-loop control (Lubarsky *et al.* 2003; Bellows *et al.* 2008; Guan *et al.* 2019*a*), the forced response of thermoacoustic systems is characterized in terms of the acoustic response alone. In other words, the acoustic response is considered to be representative of the thermoacoustic system under external forcing. However, as we show in our study, the response of the flame to forcing is considerably different from that of the acoustic field of the combustor and, therefore, measuring the acoustic response alone may not be enough to characterize the system behaviour completely. We consider the thermoacoustic system to be a system of two mutually coupled nonlinear oscillators: the acoustic pressure (p') and the HRR ($\dot{q}'$) oscillators. During stable combustor operation, both acoustic and HRR oscillators act like damped oscillators possessing different eigenmodes. During thermoacoustic instability, both of them oscillate at the frequency of limit-cycle oscillation, which develops close to the third acoustic eigenfrequency of the combustor.

Our objective is to simultaneously investigate the effect of harmonic forcing on the acoustic pressure and HRR oscillations developed during thermoacoustic instability. We characterize the forced synchronization of acoustic pressure and HRR oscillations and show that acoustic pressure and HRR oscillations have different forced synchronization characteristics at different conditions of forcing. Previous

studies have reported quenching of limit-cycle oscillations either for $f_f < f_{n0}$ alone (Lubarsky *et al.* 2003; Bellows *et al.* 2008; Mondal *et al.* 2019) or for both $f_f < f_{n0}$ and $f_f > f_{n0}$ (Balusamy *et al.* 2015; Guan *et al.* 2019*a*). We find that asynchronous quenching of the limit-cycle oscillation is attained when the forcing frequency is in the vicinity of the preferred mode (f_q) of the flame, which is lower than f_{n0} in our system. Thus, the inherent flame response plays a significant role in controlling the quenching characteristics of thermoacoustic instability in the system. Asynchronous quenching results in a 92 % drop in p'_{rms} and greater than 99 % drop in the spectral amplitude of acoustic pressure oscillations ($|\widehat{p}(f_{n1})|$). In addition, quenching can be achieved by forcing amplitudes which are just 10 % of the amplitude of limit-cycle oscillations.

We also present a systematic discourse on how the coupling between p' and $\dot{q}'$ is affected as forcing parameters are changed. We further quantify the same using the variation in phase-locking value (PLV), a measure that quantifies the synchronization behaviour of coupled oscillators (2.2), between p' and $\dot{q}'$ as a function of the forcing frequency. We find that under some forcing conditions, p' and $\dot{q}'$ undergo a transition to period-2 oscillations, somewhat similar to what had been predicted in a prior numerical study by Kashinath *et al.* (2018).

The rest of the paper is organized as follows. In § 2, we introduce the experimental set-up and the methodology. In § 2.3, we characterize the forced response of the combustor during stable operation, and the stable flame in unconfined and confined state. In § 3.1, we discuss the forced response of themoacosutic oscillations. In §§ 3.2 and 3.3, we focus exclusively on the forced synchronization of p' and $\dot{q}'$, respectively. In § 3.4, we consider the effect of forcing on the coupling between p' and $\dot{q}'$. In § 3.5, we show the possibility of period-2 behaviour of p' and $\dot{q}'$ arising due to forcing. Finally, we present the conclusions from the study in § 4.

2. Methodology

2.1. *Experimental set-up and measurements*

The experiments were conducted using a laminar combustor capable of supporting multiple flames, as shown in figure 1. Such an arrangement was originally utilized by Matsui (1981) for flame transfer function measurements, and used more recently by Kabiraj *et al.* (2012*a*) for illustrating the different dynamical states possible in a thermoacoustic system. In this set-up, the burner tube is enclosed by a glass duct whose bottom end is acoustically closed, and the top end is acoustically open to the atmosphere. The glass tube and the burner tube are of equal length, $L = 800$ mm. The glass duct has an inner diameter of 50 mm, while the burner tube has an inner diameter (d_b) of 16 mm. On the burner tube, a copper plate with seven holes is mounted. The height of the copper plate is 20 mm. The diameter (d) of each of these seven holes is 2 mm (upper inset of figure 1). Premixed conical flames are anchored on these holes (see lower inset of figure 1). A fine wire mesh is kept on the perforated copper plate to stabilize the flame.

The flame location (x_f) inside the glass duct can be varied using a traverse mechanism, having a least count of 1 mm, attached to the glass tube. The height of the flame is around $H_f = 6$ mm (see figure 1). The flame is quite small in comparison to the duct length $H_f/L = 6/800 \sim O(10^{-3})$ and the acoustic wavelength $H_f/\lambda = 6/1067 \sim O(10^{-3})$. Here, λ is the wavelength of the third acoustic eigenmode, which is $\lambda = 4L/3 = 1067$ mm. In other words, the flame is compact, and hence we use the burner surface location from the open end of the glass tube to be representative of the flame location x_f throughout this study.

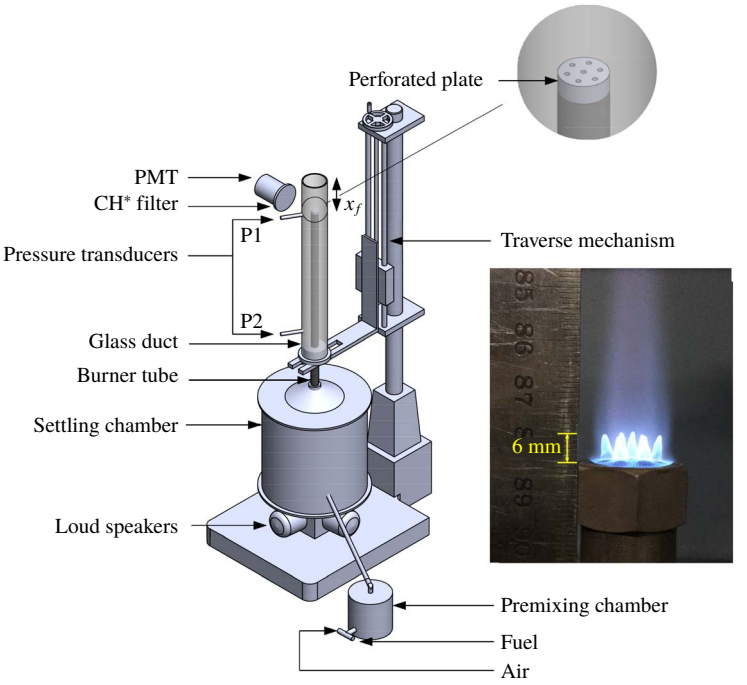

FIGURE 1. Schematic of the laminar burner with which forcing experiments were conducted. Insets show the geometry of the burner exit where the flames are anchored and an actual flame image during stable operation. There are seven conical flames whose height during stable combustion is $H_f \approx 6$ mm.

The burner tube is connected to a settling chamber with diameter $D = 223$ mm. As $D/d_b = 13.94$ (or $A_D/A_{d_b} = 194.25$, where A is the cross-sectional area), the transmission coefficient ($\mathcal{T}$) of the acoustic waves to travel from the burner tube to the settling chamber can be calculated as $\mathcal{T} = 4A_D A_{d_b}/(A_D + A_{d_b})^2 \sim 0.02$ (equation 10.10.8 from Kinsler *et al.* (1999)). Thus, the transmission coefficient is quite low. Further, the air and liquefied petroleum gas (40 % propane and 60 % butane by volume) are mixed in a premixing chamber which is connected to the settling chamber through a braided hose of diameter 2 mm. The transmission coefficient of the connection from the settling chamber to the inlets of air and fuel supply line is also quite low. Thus, we can be reasonably assured that the settling chamber prevents acoustic waves from travelling upstream of the combustion chamber to the fuel and air supply connections and causing fluctuations in the equivalence ratio.

Air and liquefied petroleum gas flow rates were maintained constant at $\dot{m}_a = 5.8$ slpm and $\dot{m}_f = 0.2$ slpm using Alicat MCR 100 slpm and Alicat MCR 10 slpm mass flow controllers throughout the experiments, respectively. The uncertainty levels are ± 0.8 % of the controlled reading and ± 0.2 % of the full-scale flow measurements. The equivalence ratio (ϕ) for this flow condition is 0.53. The thermal power of the laminar combustor is approximately 290 W. The nominal velocity at the exit of the burner tube is $\bar{U} = 4.55$ m s^{-1}. The cold-flow Reynolds number based on the diameter of the perforations is $Re_d = 583$. The maximum uncertainty in the indicated values of ϕ is ± 1.6 %, and for $\bar{U}$ and Re_d it is ± 0.8 %.

Pressure measurements were acquired using two PCB 103B02 pressure transducers mounted at a distance of 200 mm from the open end and 50 mm from the closed end of the glass duct, as indicated by P1 and P2, respectively, in figure 1. The sensitivity and resolution of the two pressure transducers are 217.5 mV kPa^{-1} and 0.2 Pa, respectively. The uncertainty in pressure measurements is ± 0.15 Pa. The HRR is measured using a Hamamatsu H5784 photomultiplier tube (PMT) equipped with a CH^* filter. The CH^* filter has a bandwidth of 10 nm and is centred around 431.4 nm to capture the photons emitted by CH^* radicals in the flame. The PMT measures the global HRR of all seven flames anchored on top of the burner tube. The pressure transducer and PMT measurements were acquired using a 16-bit NI USB 6343 data acquisition system at a sampling frequency of 10 kHz. The acoustic pressure measurements presented in the paper are from the transducer located at P1 so that the simultaneous measurements of p' and $\dot{q}'$ were acquired at the same location, and there is no artificially introduced phase delay between them. Flame images were acquired using a Phantom V12.1 camera at a framing rate of approximately ten times the frequency of the signal we wanted to measure.

The inlet flow is harmonically perturbed using four Ahuja AU-60 PA loudspeakers connected in parallel and mounted at the bottom of the settling chamber. All the speakers have an impedance of 16 Ω and an operational frequency range of 160–7000 Hz. The speakers are connected in parallel to an Ahuja UBA-500M power amplifier and the gain is set at a value of 3 units for all the experiments. The harmonic forcing signal is generated using a Tektronix arbitrary waveform generator and input to the amplifier. With the waveform generator, we can control the amplitude (A_f, in mV) and the frequency (f_f, in Hz) of the sinusoid signal. Throughout the paper, whenever we mention the amplitude of forcing, we refer to the peak-to-peak amplitude of the sinusoidal waveform that is input to the amplifier. We force the system during the state of thermoacoustic instability at four different forcing amplitudes, 10, 30, 50 and 70 mV, in the frequency range $200 \leqslant f_f \leqslant 400$ Hz. For $A_f \geqslant 30$ mV, frequency sweeping is performed in steps of 5 Hz (or $\Delta f/f_{n0} \approx 0.014$) in the region of quenching, i.e. $0.65 < f_f/f_{n0} < 0.87$ (or $240 < f_f < 320$ Hz), and in steps of 10 Hz otherwise. Thus, we capture every transition in the system dynamics with sufficiently high certainty.

The damping in the system was measured during cold-flow experiments using an acoustic pulse. The exponential decay rate of the acoustic waves in the combustor was found to be 30.8 s^{-1}. For all experiments, we ensured that the decay remains within $\pm 10\,\%$ of the indicated value to ensure repeatability in the experiments. Also, before every experiment, the air column inside the glass duct was heated by keeping the flame at a distance of 51 cm from the open end where the combustor exhibits stable operation. We found that a heating time of approximately 15 minutes was enough for the wall temperature to saturate. The wall temperature, measured using a thermocouple attached to the glass tube at 10 cm from the open end, saturated to $T_{sat} \approx 160 \pm 5\,^{\circ}\mathrm{C}$.

During each experiment involving external forcing, the forcing signal was switched off, and the system was allowed to regain its original state of limit-cycle oscillations before embarking on the next forcing cycle at a different condition of forcing. Such caution is necessary to ensure that the system does not retain any memory of the previous forcing conditions.

The repeatability of the experiments was ensured for over 10 realizations of the experiment. Even though the parametric points where the synchronization states were achieved had some variability, the trend of the results remained the same during all trials. In other words, for a given A_f, the range of f_f/f_{n0} over which different states of forced synchronization (such as phase locking, intermittent phase locking and phase drifting) were achieved had small variations.

2.2. *Nonlinear time series analysis*

2.2.1. *Measuring frequency response*

The frequency contents of the acoustic pressure (p') or the HRR ($\dot{q}'$) signals are evaluated using the fast Fourier transform algorithm. The datasets are sampled at a frequency of 10 kHz to resolve the limit-cycle signal of 368 Hz and prevent any spectral leakage. The sampling frequency is about 27 times that of the unforced limit-cycle oscillations. We acquired about 50 000 data points or about 1840 cycles of the oscillations at any given forcing condition. The fast Fourier transform algorithm was implemented using a frequency resolution of 0.153 Hz per bin for a total of 32 768 bins.

2.2.2. *Phase-space reconstruction*

The transition to forced synchronization is characterized by reconstructing the phase space on which the dynamics of the forced system evolves. For any arbitrary initial condition, the asymptotic state of a nonlinear system evolves in the phase space to a set of numerical values which make up the attractor of the system. Thus, the topological features of the attractor quantify the asymptotic dynamics of the system.

Phase space is reconstructed using Takens' delay embedding theorem (Takens 1981). The optimum time delay is obtained using average mutual information (Fraser & Swinney 1986) and the embedding dimension on which the dynamics evolve is calculated through Cao's method (Cao 1997). The calculations of average mutual information and embedding dimension are detailed in appendix A.

The trajectories of a periodic system form a closed orbit known as a limit-cycle attractor. However, the presence of noise in the signal leads to a finite width of the limit-cycle attractor. When the system dynamics contains two or more dependent frequencies, for example, a signal containing superharmonics ($f, 2f, \ldots$) leads to a closed structure with multiple loops in phase space. The number of loops indicates the number of subharmonics that are present in the signal. In the case of a quasiperiodic signal, i.e. a signal with at least two incommensurate frequencies ($f_1/f_2 \in \mathbb{I}$, where $\mathbb{I}$ is the set of irrational numbers), the trajectory evolves on a $\mathbb{T}^2$-torus. A $\mathbb{T}^2$-torus is defined as the product of two circles, $\mathbb{T}^2 = S_1 \times S_2$, where the trajectory rotates around each of the two circles (S_1, S_2) with the two incommensurate frequencies present in the system (Nayfeh & Balachandran 2008). Thus, in the case of quasiperiodic signals, the phase-space trajectory comes arbitrarily close to its origin without actually closing on itself. The forcing frequency (f_f) reported in our study is incommensurate with the frequency of the unforced limit-cycle oscillations (f_{n0}). Hence, we get quasiperiodic dynamics whenever the amplitude of forcing is not high enough to cause forced synchronization.

2.2.3. *Instantaneous phase calculation*

In order to examine the synchronization between any two given oscillators, determination of the instantaneous phase of each signal becomes important. All the signals that we consider here are periodic and narrowband in nature. Thus, the sufficient conditions are fulfilled for utilizing the concept of analytic signal introduced by Gabor (1946). We construct a complex analytic signal $\zeta(t)$ from a scalar signal $x(t)$, such that $\zeta(t) = x(t) + i\mathcal{H}[x(t)] = A(t)\mathrm{e}^{\mathrm{i}\phi(t)}$, where $\phi(t)$ is the instantaneous phase and $A(t)$ is the instantaneous amplitude of the analytic signal. Here $\mathcal{H}$ refers to the Hilbert transform, which is defined as

$$\mathcal{H}[x(t)] = \mathrm{PV}\ \frac{1}{\pi}\int_{-\infty}^{\infty}\frac{x(\tau)}{t-\tau}\,\mathrm{d}\tau. \tag{2.1}$$

Here, the integral is evaluated for the Cauchy principal value (PV). The instantaneous phase difference between two signals, $x_1(t)$ and $x_2(t)$, is then evaluated as $\Delta\phi_{x_1,x_2}(t) = \phi_{x_1}(t) - \phi_{x_2}(t)$. Synchronization of x_1 with x_2 is achieved when the relative phase between them becomes bounded to a small interval μ ($< 2\pi$) around some mean value C; i.e. $|\Delta\phi_{x_1,x_2}(t) - C| \leqslant \mu$ (Pikovsky & Maistrenko 2012). If the unwrapped relative phase between any two signals shows unbounded and monotonic increase/decrease in time, the signals are said to be desynchronized, and the trend of increasing/decreasing phase difference is termed as phase drifting.

Note that for calculating the relative phase of p' or $\dot{q}'$ with forcing, we use a reference sinusoidal signal of unit magnitude having the same frequency as that of the forcing f_f. Therefore, the temporal evolution of the relative phase of p' or $\dot{q}'$ with forcing is meaningful, but the actual value is arbitrary. Accordingly, we make all our observations of forced synchronization of acoustic and HRR oscillations based on the trend that the time evolution of the relative phase follows.

2.2.4. *Phase-locking value*

We calculate the PLV in order to quantify the synchronization between two signals. The PLV is defined as the absolute value of the mean phase difference between two signals where the instantaneous phase differences ($\Delta\phi$) are expressed as complex unit-length vectors, i.e. $e^{i\Delta\phi}$ (Lachaux *et al.* 1999; Mondal, Pawar & Sujith 2017). Mathematically, the PLV is defined as

$$\mathrm{PLV} = \frac{1}{N}\left|\sum_{j=1}^{N} \exp(\mathrm{i}\Delta\phi_{x_1,x_2}(t_j))\right|, \tag{2.2}$$

where the phase difference at the instant t_j is $\Delta\phi_{x_1,x_2}(t_j) = \phi_{x_1}(t_j) - \phi_{x_2}(t_j)$. The PLV lies close to 0 for desynchronized signals and close to 1 for perfectly synchronized signals. For cases with partial synchronization such as intermittent phase locking, the PLV lies between 0 and 1.

2.3. *Characterization of thermoacoustic subsystems*

2.3.1. *Forced acoustic response of the combustor during stable operation*

The glass duct is acoustically open at the top (acoustic pressure $p'(x/L = 0) \approx 0$) and closed at the bottom end (acoustic velocity $u'(x/L = 1) \approx 0$). In the absence of combustion (no flame), forcing the combustor leads to resonant amplification of the forcing signal at $f_f = 109$, 326 and 543 Hz. The amplification corresponds to the frequency of the first three acoustic eigenmodes ($f_n = nc/4L$, where $n = 1$, 3 and 5, and c is the speed of sound at 300 K) of the closed–open glass duct (figure is not shown here).

We next measure the response of the acoustic pressure fluctuations to forcing during stable combustor operation (i.e. no thermoacoustic instability). When x_f, the distance of the flame from the open end, is increased, the system dynamics undergoes a subcritical Hopf bifurcation from a steady state to limit-cycle oscillation at $x_f = 187$ mm ($x_f/L = 0.23$). Upon decreasing x_f, we notice that the transition from limit-cycle oscillation to steady state happens at $x_f = 150$ mm ($x_f/L = 0.19$) through the fold point. Hence, we measure the acoustic response of the system by keeping $x_f = 140$ mm ($x_f/L = 0.18$), as this location is outside the bistable zone and forcing cannot trigger the system dynamics to the state of thermoacoustic instability. So, $x_f = 140$ mm corresponds to stable combustor operation. At this x_f,

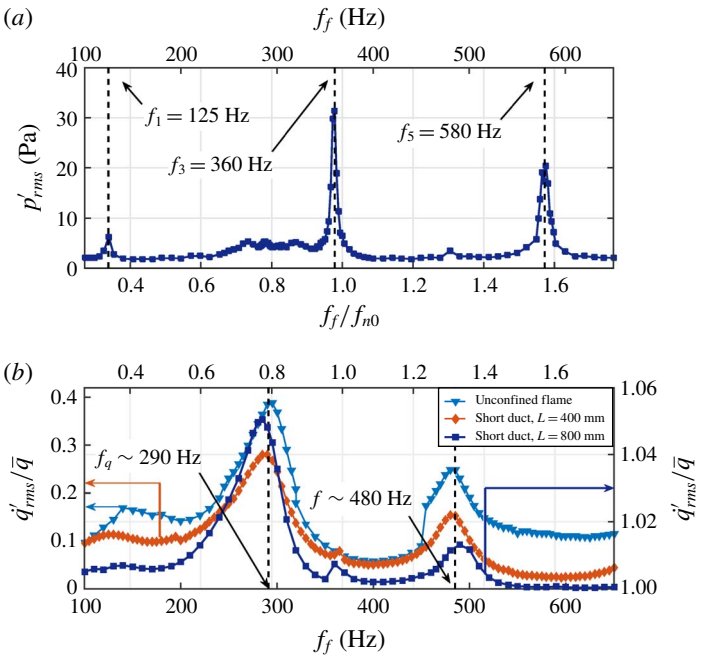

FIGURE 2. Illustration of the inherent response of different subsystems of the thermoacoustic system during stable operation. (*a*) Forced acoustic response of the long duct ($L = 800$ mm) as a function of f_f measured at the flame location $x_f = 140$ mm. (*b*) Forced response of HRR fluctuations in the flame as a function of f_f measured without confinement (▼), in a short tube (◆) ($L = 400$ mm and $x_f = 200$ mm) and in a long duct (■) ($L = 800$ mm and $x_f = 140$ mm). The amplitude of forcing is fixed at $A_f = 50$ mV for both (*a*) and (*b*). The right-hand axis in (*b*) corresponds to a larger HRR response for the case with longer duct.

the acoustic response of the duct is measured in terms of the r.m.s. value of the pressure oscillations as a function of the forcing frequency f_f and amplitude A_f. In other words, we measure $p'_{rms}(A_f, f_f) = \sqrt{\langle p'(t)^2 \rangle}$, where $p'(t)$ is the mean subtracted signal measured after external forcing has been set at a fixed value of f_f and A_f, and $\langle \cdot \rangle$ indicates time-averaged quantity.

In figure 2(*a*), we plot $p'_{rms}(A_f, f_f)$ as a function of f_f at $A_f = 50$ mV. The forcing frequency is normalized by the frequency of the unforced limit-cycle oscillations $f_{n0} = 368$ Hz obtained when x_f is fixed at 200 mm. The resonant amplification of forcing is visible for the first ($f_1 = 125$ Hz), third ($f_3 = 360$ Hz) and fifth ($f_5 = 580$ Hz) harmonics of the glass duct, which correspond to the first three acoustic eigenmodes of the stable combustor.

2.3.2. *Forced HRR response of the stable flame*

We ascertain the stability of the flame by subjecting it to forcing in unconfined and confined conditions. The premixed flame remains linearly stable to low-amplitude perturbations for all lean operating conditions. Forcing the flame at higher amplitudes ($A_f > 50$ mV) does not trigger the flame to self-excited oscillations, indicating its

nonlinear stability (Huerre & Monkewitz 1990). Consequently, we do not consider the flame to be a self-sustained oscillator but a damped harmonic oscillator.

Next, we measure the inherent flame response to forcing in unconfined and confined conditions. We use two different glass ducts to measure the flame response in the confined condition. We use a short duct and a long duct of length $L = 400$ mm and $L = 800$ mm, respectively. For the longer tube, we measure the flame response during stable operation with the flame location from the open end at $x_f = 140$ mm, as discussed previously. We repeat the same experiment by keeping $x_f = 200$ mm for a short duct of $L = 400$ mm to verify the response measured for the unconfined flame and the confined flame inside the long duct. We use the short duct because its harmonics are present at sufficiently high frequencies and forcing in the range of amplitudes and frequencies used in this study cannot trigger self-excited limit-cycle oscillations. Thus, in either of the two cases with confinement, we ensure that forcing does not trigger self-excited limit-cycle oscillations, and the measured flame response is unaffected by self-excited limit-cycle oscillations.

Keeping the location of the flame from the open end of the short duct ($x_f = 200$ mm) and long duct ($x_f = 140$ mm) constant, we perform frequency sweeping at fixed $A_f = 50$ mV. We measure $\dot{q}'_{rms}(A_f, f_f) = \sqrt{\langle \dot{q}'(t)^2 \rangle}$ for a given A_f and f_f. In figure 2(*b*), we plot the resulting flame response as a function of f_f for $A_f = 50$ mV, and normalize it with $\bar{q}$, which is the mean of the instantaneous HRR time series $\dot{q}(t)$.

We observe that the HRR response is similar for the unconfined and confined flame. We note that the HRR response is amplified for forcing frequencies close to 290 and 480 Hz (figure 2*b*). Unlike the acoustic response, the maxima in the flame response are attained at frequencies which are not integral multiples of each other, indicating the nonlinear nature of the flame. We observe that the amplification in HRR response takes place around the same frequencies for all three cases. The only difference is that the magnitude of $\dot{q}'_{rms}$ for the longer duct is about an order of magnitude greater than that for the other two cases (shown by the ordinate on the right-hand side in figure 2*b*). This difference in magnitude is possibly due to the relative location of the flame with respect to the acoustic velocity anti-node of the duct. We also notice that the increase in the amplitude of the response is not sharp but gradual, indicating that the flame is quite receptive to forcing over a broad frequency range. The flame responds well to the external forcing, showing a clear periodic response at each forcing frequency. Thus, we presume that the flame is analogous to a damped harmonic oscillator, which has preferred modes in the vicinity of $f_f = 290$ Hz and $f_f = 480$ Hz. Of these two modes, we find that the mode at 290 Hz plays a vital role in determining the frequency at which quenching of thermoacoustic instability occurs (explained further in § 3). We refer to this as the preferred mode of the flame with frequency $f_q = 290$ Hz (subscript q is used as the flame response is quantified through HRR fluctuations $\dot{q}'$). Finally, comparing the forced acoustic and HRR responses (figures 2*a* and 2*b*), we notice that the response of the stable flame is quite different from the acoustic response during stable combustor operation. Specifically, the frequencies at which the two subsystems show resonant response to forcing do not match each other.

Figure 3 depicts the variation in the flame structure of the stable flame confined inside the long duct ($L = 800$ mm) for $x_f = 140$ mm, and subjected to forcing at the frequency of preferred mode of the flame at $f_f = f_q = 290$ Hz and at the third harmonic of the duct at $f_f = f_3 = 360$ Hz. We contrast the flame dynamics at the frequency of the preferred mode, which is the parametric location of optimal quenching of thermoacoustic instability, and the frequency at which limit-cycle oscillations develop when x_f is changed. We plot the time series of the height of

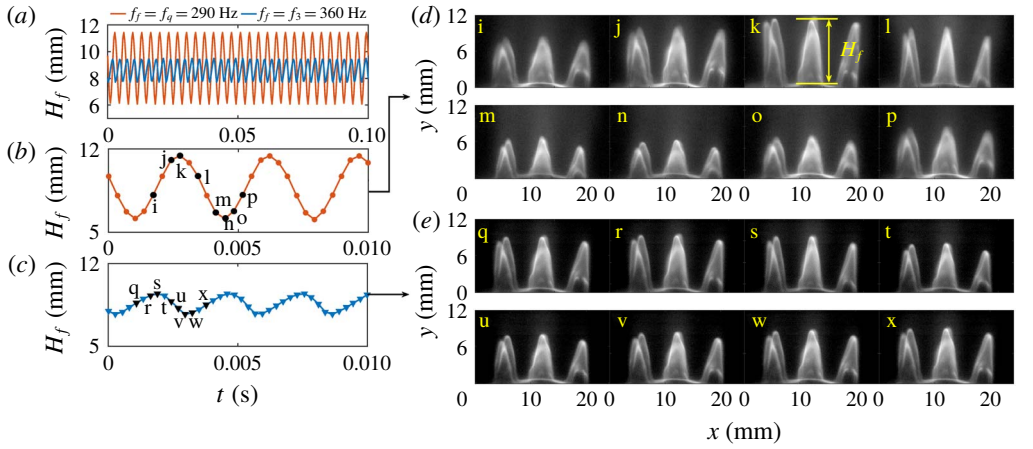

FIGURE 3. Dynamics of the stable flame when subjected to forcing at different forcing frequencies measured for the long duct ($L = 800$ mm and $x_f = 140$ mm). (*a–c*) Time series of the height of the central flame (H_f) when subjected to forcing at $f_f = f_q = 290$ Hz and $f_f = f_3 = 360$ Hz at constant $A_f = 50$ mV. Enlarged portion of the H_f time series for (*b*) $f_f = 290$ Hz and (*c*) $f_f = 360$ Hz. (*d*,*e*) Instantaneous flame images corresponding to the points marked in the time series in (*b*,*c*).

the flame (H_f) in figure 3(*a–c*). We consider the height of the flamelet at the centre to be representative of the height of the flamelets (indicated in figure 3*d*). The mean height of the flame for $f_f = 290$ Hz is $\bar{H}_f = 8.8$ mm and for $f_f = 360$ Hz is $\bar{H}_f = 8.6$ mm (figure 3*a*). The mean height of the flame is approximately the same for $f_f = 290$ and 360 Hz. However, the fluctuations in the flame height are much more pronounced for $f_f = 290$ Hz. These fluctuations in the flame height are visible quite clearly from the instantaneous flame images over a cycle of forcing as shown in figure 3(*d*). In contrast, the fluctuations are not readily apparent when the flame is forced at $f_f = 360$ Hz, as shown in figure 3(*e*). The large fluctuations in flame height or, equivalently, flame area when $f_f = f_q$ manifest in the amplification of the HRR response observed in figure 2(*b*) for f_f in the vicinity of f_q. This fact further corroborates that the preferred mode of the flame indeed exists at $f_f = f_q \approx 290$ Hz and is disparate from the acoustic frequencies of the combustor.

2.3.3. *Characteristics of self-excited limit-cycle oscillations*

The self-excited response of the laminar combustor used in the present study due to a variation in the flame location (x_f) has been characterized thoroughly by Kabiraj *et al.* (2012*a*) and Kabiraj, Sujith & Wahi (2012*b*). This system is capable of displaying a variety of dynamical states such as limit-cycle, period-k, quasiperiodic and chaotic oscillations when the location of the flame is systematically varied in the system (Kabiraj *et al.* 2012*a*,*b*). However, in the present study, we consider only the control of limit-cycle oscillation on account of it being the most commonly occurring dynamical state of unstable combustor operation. Accordingly, we set the equivalence ratio ($\phi = 0.53$) and mass flow rates ($\dot{m} = \dot{m}_a + \dot{m}_f = 6$ slpm) for which we obtain constant-amplitude limit-cycle oscillations.

As discussed previously, the system undergoes a subcritical Hopf bifurcation at $x_f = 187$ mm ($x_f/L = 0.23$) and transitions to a state of limit-cycle oscillations.

Since we obtain limit-cycle oscillations for $x_f > 187$ mm, we fix the position of the flame as $x_f = 200$ mm ($x_f/L = 0.25$) for all the experiments with open-loop forcing. The frequency of limit-cycle oscillation at $x_f = 200$ mm is $f_{n0} = 368 \pm 5$ Hz. The associated spectral amplitude of the pressure oscillations is $|\hat{p}(f_{n0})| = 105$ Pa (or 134 dB), and the r.m.s. value is $p'_{rms} \sim 140$ Pa. During thermoacoustic instability, both the acoustic pressure and HRR oscillate at f_{n0}. The frequency of the limit-cycle oscillations corresponds to the third harmonic of the closed–open duct. The small increase in the eigenfrequency of the system from 360 Hz when $x_f = 140$ mm (see figure 2*a*) to 368 Hz at $x_f = 200$ mm is expected as a larger portion of the glass duct is heated along with very large fluctuations in the HRR due to thermoacoustic instability. As a result, there is an increase in the speed of sound inside the duct, which leads to an increase in the frequency of the eigenmodes of the combustor (Sujith, Waldherr & Zinn 1995).

3. Results and discussion

As mentioned earlier, we measure the forced response of thermoacoustic oscillations by keeping the flame location fixed at $x_f = 200$ mm ($x_f/L = 0.25$), where there are strong self-excited limit-cycle oscillations with frequency $f_{n0} = 368 \pm 5$ Hz and $p'_{rms} \sim 140$ Pa. Once the limit-cycle oscillations are stabilized, the forcing parameters (amplitude, A_f, and frequency, f_f) are systematically altered, leaving all the other control parameters (such as flame location, x_f, and equivalence ratio, ϕ) unchanged.

3.1. *Forced response of thermoacoustic oscillations*

Figure 4 shows the response of thermoacoustic instability to external forcing as a function of f_f and A_f. As before, the response is measured in terms of the r.m.s. value as it is a measure of the energy content of the signal regardless of the specific frequency content. As external forcing induces additional frequencies in the signal, measuring the response at any given frequency would only provide an incomplete picture of the response.

At a very low amplitude of forcing ($A_f = 10$ mV), the thermoacoustic system remains unaffected as indicated by the relative insensitivity of p'_{rms} and $\dot{q}'_{rms}$ to a change in f_f as shown in figures 4(*a*) and 4(*b*), respectively. On increasing the amplitude of forcing to $A_f = 30$ mV, we notice a small decrease in p'_{rms} (figure 4*a*), while $\dot{q}'_{rms}$ shows a corresponding increase in the frequency range $0.7 < f_f/f_{n0} < 0.82$. The decrease in p'_{rms} and the increase in $\dot{q}'_{rms}$ for $0.7 < f_f/f_{n0} < 0.82$ become more pronounced as we increase the forcing amplitude first to 50 mV and then to 70 mV. At $A_f = 70$ mV, we notice a maximum decrease in p'_{rms} at $f_f/f_{n0} = 0.79$. Here, we achieve about 92 % decrease in p'_{rms} from an initial unforced value of $p'_{rms} = 140$ Pa at $f_f/f_{n0} = 0$ to $p'_{rms} = 11.8$ Pa at $f_f/f_{n0} = 0.79$. The decrease in the amplitude of limit-cycle oscillations due to forcing at a frequency away from the natural frequency is referred to as asynchronous quenching (Guan *et al.* 2019*a*; Mondal *et al.* 2019). We notice that with increasing amplitude of forcing, there is a progressively greater quenching of p'_{rms} and a wider frequency range over which quenching is observed (shaded region in figure 4). In contrast, $\dot{q}'_{rms}$ shows an amplification in the frequency range $0.7 < f_f/f_{n0} < 0.82$. For both $A_f = 50$ and 70 mV, the increase in $\dot{q}'_{rms}/\bar{q}$ observed in figure 4(*b*) is quite comparable to the amplification achieved when the stable flame is forced (see figure 2*b*). Clearly, this increase in $\dot{q}'_{rms}/\bar{q}$ is analogous to the resonance observed at the frequency of the preferred mode of the stable flame in figure 2(*b*).

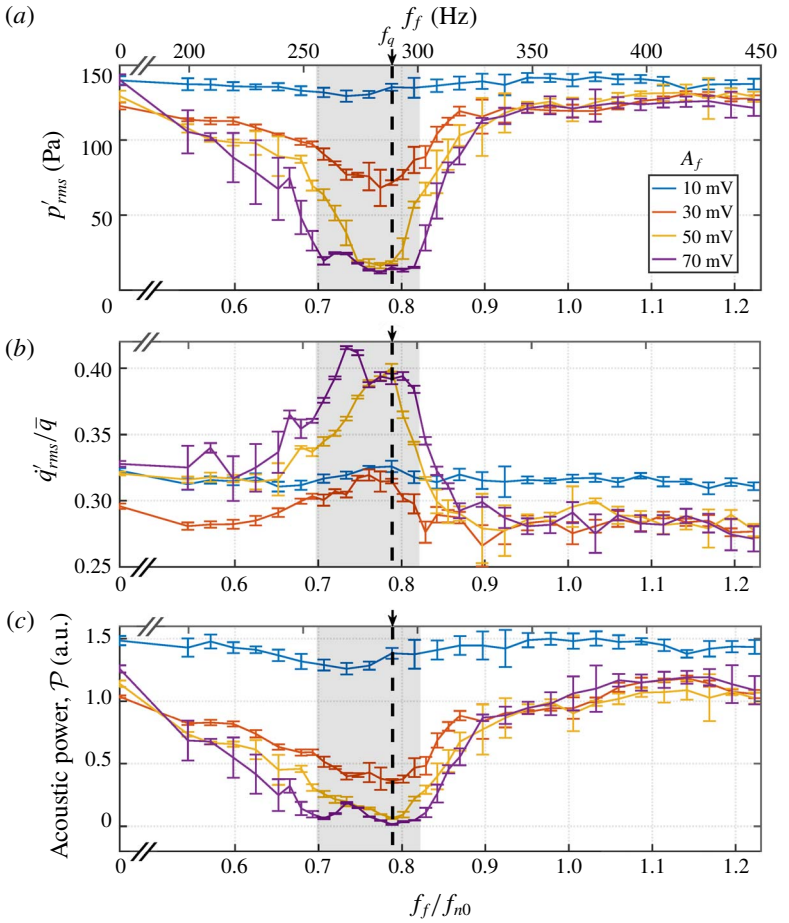

FIGURE 4. Demonstration of open-loop control of thermoacoustic instability. Response of (*a*) acoustic pressure (p'_{rms}) and (*b*) normalized HRR fluctuations ($\dot{q}'_{rms}/\bar{q}$) as a function of the normalized forcing frequency (f_f/f_{n0}). (*c*) The time-averaged acoustic power production, $\mathcal{P}$ (1.1), of the thermoacoustic system as a function of the normalized forcing frequency at the indicated amplitude of forcing (A_f). The shaded region indicates the region of asynchronous quenching for $A_f > 30$ mV. The axis on the top indicates f_f. The error bars represent twice the standard deviation of the time series obtained for any given f_f and A_f.

Figure 4(*c*) shows the dependence of time-averaged acoustic power production, $\mathcal{P}$ (1.1), on the forcing frequency at different A_f. Notice that $\mathcal{P}$ follows a similar trend to p'_{rms}. At low forcing amplitude, the time-averaged acoustic power production remains very high (figure 4*c*). Increase in forcing amplitude in the range $0.7 < f_f/f_{n0} < 0.82$ causes a progressively higher reduction in the magnitude of $\mathcal{P}$. So, even though there is an increase in $\dot{q}'_{rms}/\bar{q}$ for $0.7 < f_f/f_{n0} < 0.82$ (figure 4*b*), the coupling of p' and $\dot{q}'$ is such that the acoustic power production is very low and hence the system cannot sustain thermoacoustic instability. The maximum reduction in p'_{rms} is obtained at $f_f/f_{n0} = 0.79$ at which point the acoustic power production is also at its lowest, i.e. $\mathcal{P} \sim 0.01$ a.u. Thus, there is a negligible contribution of the flame to the acoustic energy in the combustor during the state of quenching of limit-cycle

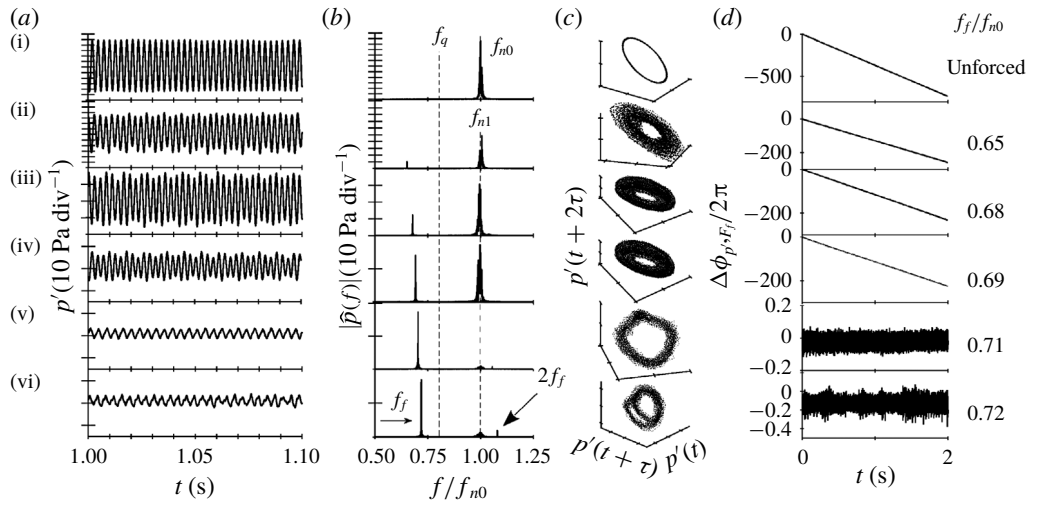

FIGURE 5. Depiction of forced synchronization of the acoustic pressure oscillations with increasing f_f at a fixed $A_f = 70$ mV. (*a*) Time series, (*b*) amplitude spectrum and (*c*) the phase portrait of the pressure fluctuations. (*d*) The time evolution of phase difference between p' and forcing, $\Delta\phi_{p',F_f}$. Dashed lines in (*b*) indicate the frequency of unforced limit cycle (f_{n0}) and preferred mode of the flame (f_q). Note that the ordinate is different for (*a*,*b*) where each division represents 10 Pa.

oscillations. At other forcing frequencies, the acoustic power production remains quite high, indicating the inefficacy of forcing to control thermoacoustic instability.

Of particular note here is that the flame significantly affects the frequency at which quenching is observed. We hypothesize that external forcing at the frequency of the preferred mode of the flame, which is disparate from the eigenfrequency of the combustor, is responsible for the asynchronous quenching of pressure oscillations in our system. One possible explanation is that as the forcing frequency is close to the preferred mode of the flame, HRR oscillations are amplified. In contrast, since the forcing frequency is far away from the frequency of acoustic eigenmode, a standing wave cannot be established inside the duct. As a result, the thermoacoustic feedback loop is disrupted, and the modified Rayleigh criterion (acoustic driving greater than damping) is not satisfied even though the amplitude of HRR oscillations are very large.

In the subsequent sections, we methodically describe the changes in the response of acoustic and HRR oscillations as the frequency or amplitude of forcing is varied systematically. We also quantify the changes in the dynamics of pressure and HRR oscillations relative to the forcing frequency by measuring the evolution of the relative phase, i.e. $\Delta\phi_{p',F}$ and $\Delta\phi_{\dot{q}',F}$. The instantaneous phase is calculated using the method of Hilbert transform (2.1) as detailed in § 2.2.3.

3.2. *Effect of forcing on the dynamics of acoustic pressure oscillations*

3.2.1. *Varying forcing frequency:* $f_f/f_{n0} = 0 \to 0.72$ *at* $A_f = 70$ mV

Figure 5 depicts the forced synchronization of p' as f_f is varied at a fixed $A_f = 70$ mV. When forcing is absent, p' is periodic with only one characteristic frequency, f_{n0} (figure 5*b*i). Increase in f_f/f_{n0} to 0.65 leads to increasingly modulated

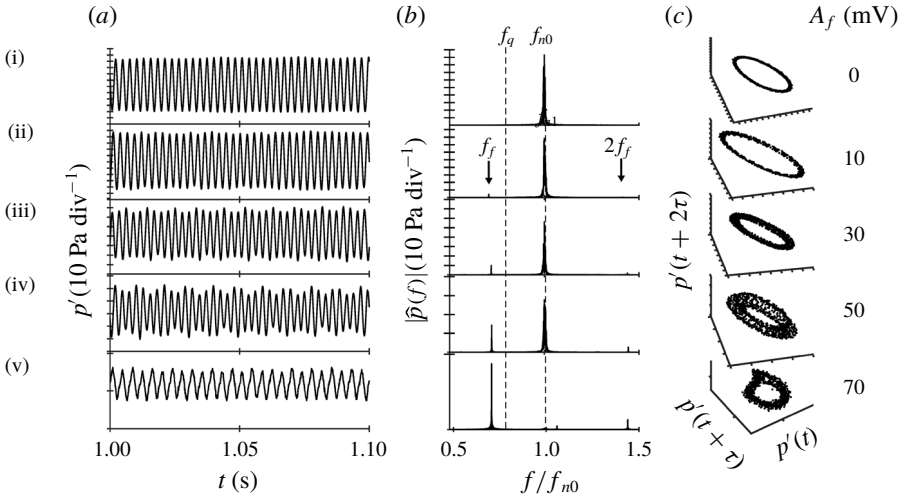

FIGURE 6. Demonstration of forced synchronization of acoustic pressure oscillations with increasing A_f at a constant $f_f/f_{n0} = 0.71$ (or $f_f/f_q = 0.9$). (*a*) Time series, (*b*) amplitude spectrum and (*c*) the phase portrait of p' for the indicated values of A_f shown in the last column. Torus-birth and torus-death bifurcations take place when A_f is increased from 10 to 30 mV and from 50 to 70 mV, respectively. Note that the ordinate is different for (*a*,*b*) where each division represents 10 Pa.

p' signal (figure 5*a*ii), indicating the presence of two incommensurate frequencies (figure 5*b*ii). Accordingly, the phase-space trajectory lies on a $\mathbb{T}^2$-torus. Such a quasiperiodic behaviour persists for $0.68 < f_f/f_{n0} < 0.71$. In this range of f_f/f_{n0}, the spectral amplitude of forcing is lower but comparable to the amplitude of limit-cycle oscillations at f_{n1} (see figure 5*b*iii,iv). Here, f_{n1} is the response frequency of the limit-cycle oscillations to forcing. We notice that the spectral amplitude of limit-cycle oscillations at f_{n1} continues to decrease (see the transition from figures 5*b*iii to 5*b*iv). For $f_f/f_{n0} < 0.71$, the unwrapped relative phase between the acoustic pressure oscillations and forcing ($\Delta\phi_{p',F_f}$) shows unbounded and monotonic variation in time (figures 5*d*ii–5*d*iv), indicating desynchronized nature of the signals.

For $f_f/f_{n0} = 0.71$ and 0.72, the spectral amplitude of p' at f_{n1} (figure 5*b*v,vi) decreases to $\sim$99 % of the unforced spectral amplitude. This corresponds to $\sim$80 % decrease in p'_{rms} from the unforced value, as can be observed from figure 4(*a*). We further observe a transition from a state of phase drifting (figure 5*d*iv) to phase locking (figure 5*d*v) in the relative phase plot between pressure and forcing signals. Recall from § 1.2 that forced synchronization is said to be achieved if the forcing frequency is the only characteristic frequency in the signal and the instantaneous relative phase between the response and forcing becomes bounded to 2π. Thus, at $f_f/f_{n0} = 0.71$, the acoustic pressure oscillations associated with limit-cycle oscillations have undergone forced synchronization.

3.2.2. *Varying forcing amplitude:* $A_f = 0 \rightarrow 70$ mV *at* $f_f/f_{n0} = 0.71$

Next, we characterize the forced synchronization of acoustic pressure oscillations as the forcing amplitude is increased at a fixed forcing frequency $f_f/f_{n0} = 0.71$. At $A_f = 0$, we notice the characteristic frequency (f_{n0}) of limit-cycle oscillations in the amplitude spectrum (figure 6*b*i) and the associated single closed-loop attractor (figure 6*c*i).

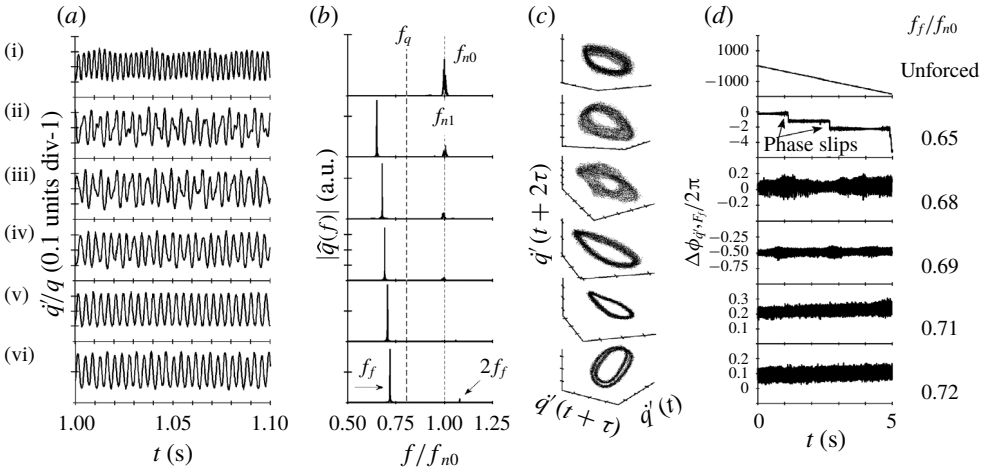

FIGURE 7. Transition to forced synchronization of the HRR oscillations for increasing f_f at fixed $A_f = 70$ mV. (*a*) Time series, (*b*) amplitude spectrum and (*c*) the phase portrait of the normalized HRR fluctuations measured for the indicated values of forcing frequency. (*d*) Time evolution of phase difference between $\dot{q}'$ and the forcing, $\Delta\phi_{\dot{q}',F_f}$.

An increase in A_f to 30 mV leads to a transition from limit-cycle to quasiperiodic dynamics (figure 6*c*iii). The acoustic response remains quasiperiodic with further increase in forcing amplitude (figures 6*c*iii,6*c*iv). Finally, at $A_f = 70$ mV, we notice that there is only one characteristic frequency (f_f) in the system (figure 6*b*v) and the relative phase becomes bounded (figure 5*d*v), indicating the forced synchronization of p'.

Thus, in either of the two cases $f_f/f_{n0} = 0 \rightarrow 0.72$ at $A_f = 70$ mV and $A_f = 0 \rightarrow 70$ mV at $f_f/f_{n0} = 0.71$, the dynamics of pressure oscillations transitions from limit cycle at f_{n0} to quasiperiodicity with frequency f_{n1} and f_f, and back to limit cycle at f_f. The associated bifurcations are: limit cycle to quasiperiodic through torus-birth bifurcation, and quasiperiodic to limit cycle through torus-death bifurcation (Balanov *et al.* 2008; Li & Juniper 2013*b*; Kashinath *et al.* 2018).

3.3. *Effect of forcing on the dynamics of HRR oscillation*

Now, we characterize the response of the HRR oscillations when subjected to forcing at constant $A_f = 70$ mV. Figure 7 shows the transition in the response of HRR as f_f is increased. In the absence of forcing ($f_f/f_{n0} = 0$), we observe that the dynamics of HRR has a narrowband peak at f_{n0} (figure 7*b*i). However, the time series of this signal exhibits visible modulations (figure 7*a*i). Such modulations could be a result of the low flame intensity, making the signal highly susceptible to ambient noise. Consequently, the phase-space trajectory appears to be scattered about the limit-cycle attractor (figure 7*c*i).

At $f_f/f_{n0} = 0.65$, we observe that the spectral amplitude of HRR oscillations at f_f is larger than but comparable to the spectral amplitude at f_{n1} (i.e. $\hat{q}(f_f) > \hat{q}(f_{n1})$; figure 7*b*ii). The presence of these incommensurate frequencies in the spectrum results in the existence of a distinct $\mathbb{T}^2$-torus in the phase space, indicative of the quasiperiodic nature of HRR oscillations (figure 7*c*ii). At this f_f, forcing also leads to phase locking of HRR signal with random phase slips interspersed in it (figure 7*d*ii).

Here, phase slips refer to jumps in the mean value of the phase difference between $\dot{q}'$ and forcing in integer multiples of 2π radians, as indicated in figure 7(*d*ii). This is referred to as intermittent phase locking of the forcing and HRR oscillations.

For $f_f/f_{n0} = 0.68$, the spectral amplitude of HRR oscillations at f_{n1} is very low in comparison to the spectral amplitude of forcing at f_f (figure 7*b*iii). Figure 7(*d*iii) shows that the HRR oscillations are phase-locked to forcing, indicating the occurrence of forced synchronization of HRR oscillations in the system. Increase in forcing frequency ($f_f/f_{n0} > 0.68$) leads to a progressive decrease in the spectral amplitude of HRR fluctuations at f_{n1} to the point where it completely disappears at $f_f/f_{n0} = 0.71$ (figure 7*b*v).

The transition of HRR oscillations from the unforced limit cycle at f_{n0} to limit-cycle oscillations at f_f during the process of forced synchronization follows a similar change to that undergone by the acoustic pressure oscillations (figure 5). However, the frequency range over which $\dot{q}'$ is synchronized to forcing is larger than that for p'. Similarly, the transition in the dynamics of HRR oscillations for an increase in A_f at a given f_f is similar to the acoustic response plotted in figure 6 but has not been shown here for brevity. The only difference is that for a given f_f, $\dot{q}'$ undergoes forced synchronization at a lower A_f than p' does. A possible explanation for such an occurrence might be the fact that the flame is more receptive to the external harmonic forcing whenever the forcing frequency is close to the frequency of the preferred mode of the flame.

Recently, in an electrically heated horizontal Rijke tube, Mondal *et al.* (2019) showed that when pressure oscillations are forced at a frequency close to f_{n0}, there is a quenching of the spectral amplitude of pressure oscillations at f_{n1} due to synchronization, while the spectral amplitude at f_f undergoes resonant amplification. As a result, they observed high amplification in the r.m.s. value of acoustic pressure oscillations, which they referred to as synchronance (synchronization–resonance). We observe similar behaviour in our system. The forced synchronization of HRR oscillations around f_q (figure 7v,vi) is observed simultaneously with the enhancement in $\dot{q}'_{rms}$ (figure 4*b*). Thus, we possibly observe synchronance in the HRR oscillations at $f_f = f_q$.

The combined forced synchronization of acoustic pressure and HRR oscillation is quite important. We observe only small reductions in the amplitude of p' when only $\dot{q}'$ is synchronized to forcing (for $f_f/f_{n0} < 0.7$ in figure 4*a*). We notice a very high reduction in the amplitude of thermoacoustic instability when both p' and $\dot{q}'$ undergo forced synchronization at $f_f/f_{n0} = 0.72$ in figure 4(*a*). In some of the previous studies (Balusamy *et al.* 2015; Kashinath *et al.* 2018; Guan *et al.* 2019*a*; Mondal *et al.* 2019), the forced synchronization of acoustic pressure is observed around the acoustic eigenfrequency of the combustor. In contrast, we find that the forced synchronization of the two oscillators takes place around the frequency of the preferred mode of the flame instead of the acoustic eigenfrequency. Thus, we conclude that the flame exerts significant control on the dynamics of asynchronous quenching and forced synchronization characteristics of the limit-cycle oscillations.

3.4. *Effect of forcing on the coupling between the acoustic and HRR oscillations*

Here, we assess and quantify the effect of forcing on the mutual coupling of the acoustic pressure and HRR oscillations. Figure 8 displays the time-averaged acoustic power production, $\mathcal{P}$, as a function of the forcing frequency at fixed $A_f = 70$ mV. The associated time evolutions of the phase difference ($\Delta\phi_{p',\dot{q}'}(t)$) between the acoustic

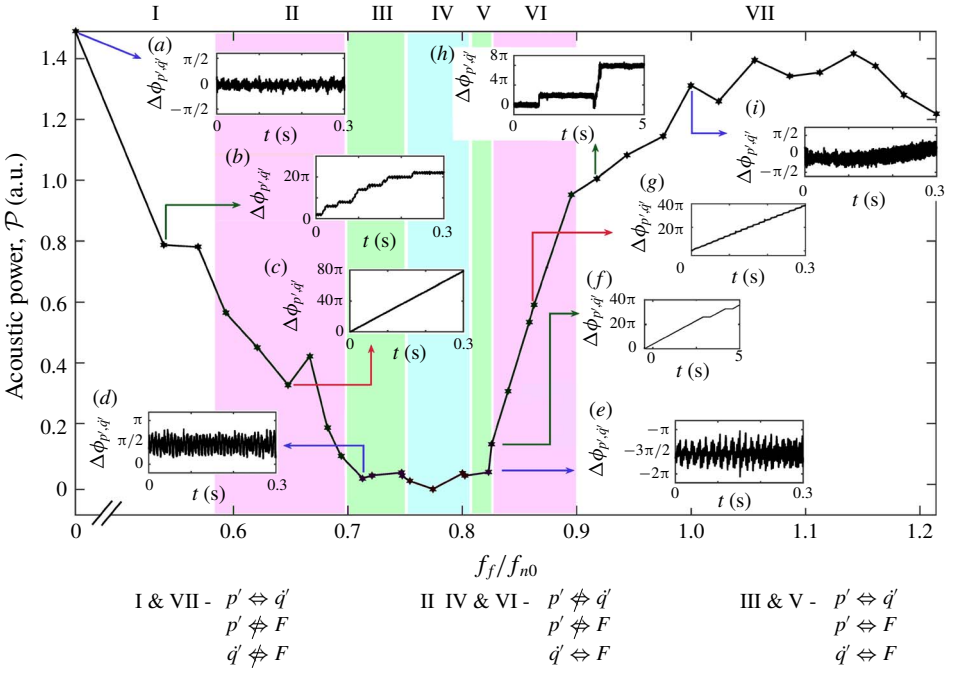

FIGURE 8. Effect of forcing on the mutual coupling between acoustic pressure and HRR oscillations. The time-averaged acoustic power production ($\mathcal{P}$) is plotted as a function of the normalized forcing frequency f_f/f_{n0} at $A_f = 70$ mV. The insets (*a–g*) indicate the time evolution of $\Delta\phi_{p',\dot{q}'}$ (in radians) at the indicated forcing frequencies. The inter-relationship among p', $\dot{q}'$ and F is indicated below the figure. The symbol '$\Leftrightarrow$' indicates that a state of synchronization exists between any two given oscillators, while '$\not\Leftrightarrow$' indicates that the two oscillators remain desynchronized.

pressure and HRR oscillations are also shown at different forcing frequencies. In thermoacoustic systems in general, the coupling between p' and $\dot{q}'$ is asymmetric and nonlinear (Godavarthi *et al.* 2018). Thus, the quantification of the response of the coupling between p' and $\dot{q}'$ to external forcing is of particular significance.

The effect of forcing on the system has been divided into seven regions depending upon the inter-relationship between the three oscillators: p', $\dot{q}'$ and F. In figure 8, we indicate the existence of some form of synchronization among each of the oscillators with '$\Leftrightarrow$'. These states of synchronization are either the state of forced synchronization or state exhibiting partial synchronization such as intermittent phase locking. The desynchronization between any two given oscillators is indicated with '$\not\Leftrightarrow$'. Thus, regions I and VII correspond to states where only p' and $\dot{q}'$ are mutually synchronized. In regions II–VI, $\dot{q}'$ and forcing remain synchronized, while p' is synchronized to forcing only in regions III and V. In regions III and V, all three oscillators are synchronized to each other.

In region I, the effect of forcing is negligible. Therefore, forcing cannot affect the coupling between p' and $\dot{q}'$, and the relative phase between p' and $\dot{q}'$ oscillates around a mean ($\overline{\Delta\phi_{p',\dot{q}'}}$) of $-2.1°$ and a standard deviation of $\pm 9.4°$, which is equivalent to p' and $\dot{q}'$ being nearly in phase with each other (figure 8*a*). Thus, there is a net positive acoustic driving in the system and the acoustic power production is quite high ($\mathcal{P} = 1.49$ a.u.). For $f_f/f_{n0} < 0.58$, forcing can only cause intermittent phase slips in

the state of phase locking between p' and $\dot{q}'$ (figure 8*b*). Each of the remaining pair of oscillators, p'–forcing and $\dot{q}'$–forcing, remain desynchronized.

For f_f/f_{n0} in the range 0.58–0.69 (region II), we notice that forcing causes disruption in the coupling between p' and $\dot{q}'$, and $\Delta\phi_{p',\dot{q}'}$ shows unbounded and monotonic growth (figure 8*c*). In this region, forced synchronization of $\dot{q}'$ is established (see figures 7*d*ii–7*d*iv). However, the net forcing amplitude is still insufficient to cause forced synchronization of p', as can be seen from the phase drift in the relative phase plot in figures 5(*d*ii)–5(*d*iv).

Regions III, IV and V together constitute the frequency range over which we observe a significant quenching of limit-cycle oscillations for $A_f > 30$ mV (as shown in figure 4). In region III, both p' and $\dot{q}'$ exhibit phase locking with forcing (figures 5*d*v and 6*d*v). Consequently, phase locking between p' and $\dot{q}'$ (see figure 8*d*) is established. The relative phase between p' and $\dot{q}'$ oscillates about $\overline{\Delta\phi_{p',\dot{q}'}} = 81.5° \pm 22.6°$. Thus, the pressure and the HRR oscillations are nearly $\pi/2$ rad out of phase with each other. As a result, there are alternate cycles of acoustic driving (when $\Delta\phi_{p',\dot{q}'} < \pi/2$) and damping (when $\Delta\phi_{p',\dot{q}'} > \pi/2$) in the system such that there is a positive but very low value of net acoustic power production, $\mathcal{P} = 0.02$ a.u.

In region IV, only $\dot{q}'$ is synchronized with forcing. This is due to period-2 dynamics of the pressure oscillations. We elaborate on the period-2 dynamics in p' and $\dot{q}'$ further in § 3.5. Region V is akin to region III and each of the three oscillators remain synchronized. At this point, the relative phase between p' and $\dot{q}'$ is observed to oscillate about $\overline{\Delta\phi_{p',\dot{q}'}} = -277.1° \pm 25° \sim -3\pi/2 \equiv \pi/2$ rad (figure 8*e*). The time-averaged normalized power production is again very low with $\mathcal{P} = 0.04$ a.u.

For $0.82 < f_f/f_{n0} < 1$ (regions V, VI and VII), the impact of forcing on the dynamics of the acoustic pressure and HRR oscillations progressively decreases. In this range of f_f, we notice that the $\Delta\phi_{p',\dot{q}'}$ transitions from a state of phase locking at about $\sim\pi/2$ rad (at $f_f/f_{n0} = 0.82$ in figure 8*e*), to intermittent phase locking (at $f_f/f_{n0} = 0.83$ in figure 8*f*), to phase drifting (at $f_f/f_{n0} = 0.85$ in figure 8*g*), to intermittent phase locking (at $f_f/f_{n0} = 0.93$ in figure 8*h*) and, finally, to in-phase locking (at $f_f/f_{n0} = 1$ in figure 8*i*). At $f_f/f_{n0} = 1$, the relative phase between p' and $\dot{q}'$ oscillates about $\overline{\Delta\phi_{p',\dot{q}'}} = 13° \pm 18.8° \sim 0$ (figure 8*g*). Thus, p' and $\dot{q}'$ are in phase and result in maximum acoustic driving, leading to a very high acoustic power production, $\mathcal{P} = 1.3$ a.u.

We next quantify the effect of forcing on the coupled behaviour of pressure and HRR oscillations. We use PLV to measure the extent of phase locking between the acoustic and HRR oscillations during forcing as defined in (2.2).

Figure 9 plots PLV between the pairs of signals p'–$\dot{q}'$, p'–F and $\dot{q}'$–F as a function of the forcing frequency at $A_f = 70$ mV. The PLV of p'–$\dot{q}'$ corresponds quite well with the phase-locking characteristics seen in figure 8. For $f_f/f_{n0} < 0.68$, there is an almost monotonic drop in the PLV of p'–$\dot{q}'$. The decrease in PLV is a result of the presence of desynchronized quasiperiodic dynamics in both p' and $\dot{q}'$. The PLV of p'–$\dot{q}'$ increases to a very high value for $0.72 < f_f/f_{n0} < 0.75$, indicating the relatively high synchronized behaviour between them (figure 8*d*). Following this, we observe a drop in the PLV of p'–$\dot{q}'$. The drop occurs due to the existence of different dynamics in both p' and $\dot{q}'$, where p' has period-2 dynamics (figure 10*b*iii) and $\dot{q}'$ has limit-cycle dynamics (figure 10*d*iii). This results in phase drifting in their relative phase (figure 10*e*iii), and, thus, the low value of PLV between them (discussed further in § 3.5). For $0.85 < f_f/f_{n0} < 1.2$, the PLV of p'–$\dot{q}'$ increases and reaches a value very close to 1 because the forcing becomes ineffective to disrupt the mutual coupling of p' and $\dot{q}'$.

The PLV between p' and F is also consistent with our observations in § 3.2. It attains a very low value for frequencies where the forcing is insufficient to cause

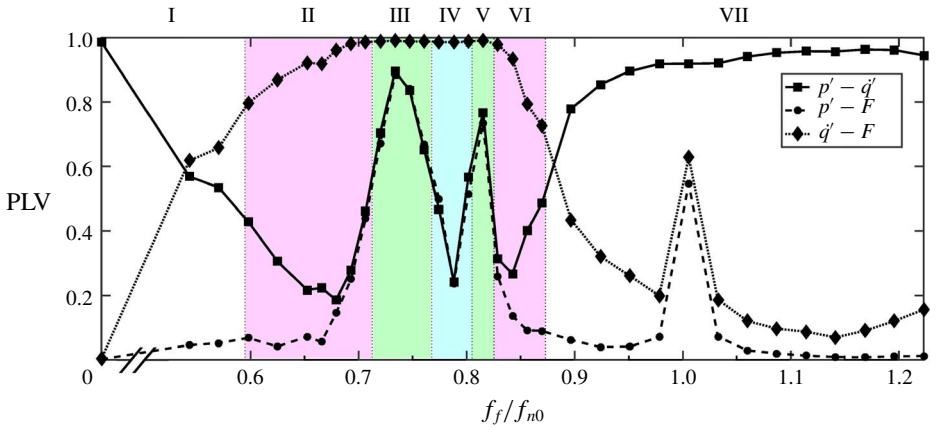

FIGURE 9. Quantifying the effect of forcing on the mutual coupling between acoustic and HRR oscillations. The PLV is plotted as a function of the normalized forcing frequency for $A_f = 70$ mV. Refer to figure 8 for the demarcation of regions I–VII.

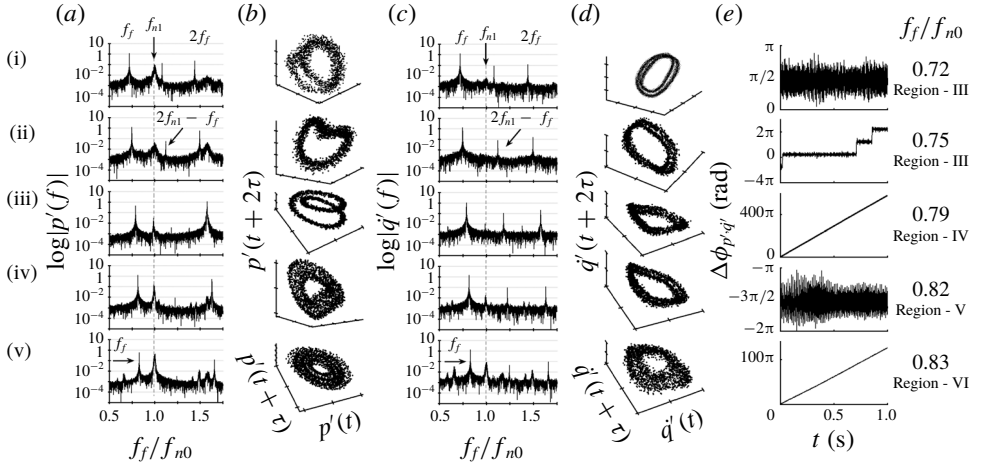

FIGURE 10. Plot depicting the different dynamical states of the thermoacoustic system inside the region marked by III–VI in figure 8. (*a*,*c*) Amplitude spectrum and (*b*,*d*) phase portrait of the normalized p' and $\dot{q}'$, respectively. (*e*) The time evolution of the instantaneous relative phase plot between p' and $\dot{q}'$, i.e. $\Delta\phi_{p',\dot{q}'}(t)$, for the indicated values of f_f/f_{n0} (last column) at $A_f = 70$ mV.

forced synchronization ($0 < f_f/f_{n0} < 0.72$ and $0.82 < f_f/f_{n0} < 1.2$). Further, its value is quite high whenever forced synchronization of the acoustic response is achieved. Meanwhile, the PLV of $\dot{q}'$–F depicts the large frequency range over which forced synchronization of HRR oscillations is attained ($0.59 < f_f/f_{n0} < 0.86$). The increase in PLV at $f_f/f_{n0} = 1$ of p'–F and p'–$\dot{q}'$ is the trivial case when the forcing frequency is approximately the same as the frequency of limit-cycle oscillations, due to which we obtain phase locking between the indicated pair of oscillators.

f_f/f_{n0}	p'	$\dot{q}'$	$\Delta\phi_{p',F}(t)$	$\Delta\phi_{\dot{q}',F}(t)$	$\Delta\phi_{p',\dot{q}'}(t)$
0.71	LC	LC	PL	PL	PL at $\approx\pi/2$
0.72	P2	P2	PL	PL	PL at $\approx\pi/2$
0.75	P2	LC	IPL	PL	IPL
0.79	P2	LC	PD	PL	PD
0.82	LC	LC	PL	PL	PL at $\approx-\pi/2$
0.83	QP	QP	IPL	PL	IPL

TABLE 1. Different dynamical states of p' and $\dot{q}'$ associated with variation in the values of f_f in regions III to V of figure 8 at $A_f = 70$ mV. The dynamical states of p' and $\dot{q}'$ and the relative phase ($\Delta\phi$) are indicated for different forcing frequencies. The different dynamical states are abbreviated as: LC, limit cycle; QP, quasiperiodic; P2, period-2; PL, phase locking; IPL, intermittent phase locking; PD, phase drifting. The transition of any subsystem from one dynamical state to another with variation in forcing frequency is associated with the following bifurcations (Kuznetsov 2013): LC (figures 5v and 7v) $\rightarrow$ P2 (figure 10i) – period doubling; P2 (figure 10iii) $\rightarrow$ LC (figure 10iv) – period-halving; and LC (figure 10iv) $\rightarrow$ QP – torus-birth (figure 10v).

3.5. *Period-2 response of the system during forced synchronization*

3.5.1. *Varying forcing frequency: $f_f/f_{n0} = 0.72 \rightarrow 0.8$ at $A_f = 70$ mV*

Now, we consider the response of acoustic pressure and HRR oscillations for $0.72 < f_f/f_{n0} < 0.8$, which spans regions III–V in figures 8 and 9. At $f_f/f_{n0} = 0.72$ (in region III, figure 8*d*), there is a phase locking of p' and $\dot{q}'$ with the forcing signal (refer to figures 5*d*vi and 7*d*vi). From figure 10(*e*i), we see that p' and $\dot{q}'$ exhibit phase locking with each other. From the amplitude spectrum, we note that $|\hat{p}(2f_f)|/|\hat{p}(f_f)| \sim 10^{-1}$ (figure 10*a*i). The frequencies which are integer multiples of each other and are of comparable amplitudes manifest in the phase-space trajectory as an additional loop in the limit-cycle attractor of both p' (figure 10*b*i) and $\dot{q}'$ (figure 10*d*i). This is indicative of the period-2 nature of these signals. Other linear combinations of f_f, $2f_f$ and f_{n1} (e.g. peak at $2f_f - f_{n1}$) are also visible in the spectrum. However, the magnitudes of these additional peaks are quite small and can be ignored. As forcing frequency is increased ($f_f/f_{n0} = 0.72 \rightarrow 0.79$), the phase-space trajectory of acoustic pressure oscillations indicates period-2 oscillations more clearly (see figure 10*b*iii). The amplitude spectrum shows that the dominant frequency switches from f_f at $f_f/f_{n0} = 0.72$ to $2f_f$ at $f_f/f_{n0} = 0.79$ all the while showing period-2 dynamics in pressure oscillations. In contrast, the dynamics of HRR oscillations loses period-2 oscillations and regains limit-cycle oscillations at $f_f/f_{n0} = 0.79$ (figure 10*d*iii).

The different dynamics of p' and $\dot{q}'$ also affects their mutual coupling, as is observed from figure 10(*e*). We notice that the instantaneous relative phase plot shows a state of phase locking when both pressure and HRR oscillations have period-2 behaviour (figure 10*e*i). The state of mutual synchronization between p' and $\dot{q}'$ is lost as forcing frequency is increased. The state of phase locking transitions to intermittent phase locking (figure 10*e*ii), and finally to phase drifting (figure 10*e*iii) when acoustic pressure undergoes period-2 oscillations and HRR undergoes period-1 limit-cycle oscillations. The phase drifting between pressure and HRR oscillations is also responsible for the lowest acoustic power production ($\mathcal{P} = 0.01$) for $f_f/f_{n0} = 0.79$ in region IV (figure 8).

We summarize the dynamics of the two subsystems taking place in regions III–V of figure 8 in table 1. The transition in the dynamics is also indicated in table 1.

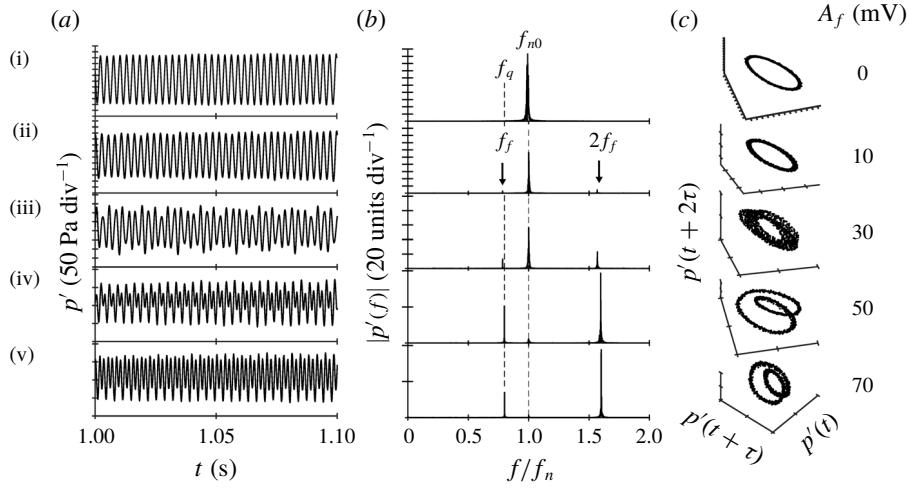

FIGURE 11. The transition from limit-cycle oscillations to period-2 acoustic oscillations as a result of the increase in the amplitude of forcing. (*a*) The time trace of p', (*b*) the amplitude spectra and (*c*) the phase portrait for A_f shown in the last column for fixed $f_f/f_{n0} = 0.79$ or equivalently at $f_f = f_q$. Torus-birth and period-doubling bifurcations take place when A_f is increased from $10 \rightarrow 30$ mV and from $30 \rightarrow 50$ mV, respectively.

For example, for $f_f/f_{n0} : 0.71 \rightarrow 0.72$, the state of p' changes from limit cycle (LC) to period-2 (P2). The bifurcation associated with this change is a period-doubling bifurcation.

3.5.2. *Varying forcing amplitude:* $A_f = 0 \rightarrow 70$ mV *at* $f_f/f_{n0} = 0.79$

Figure 11 shows the transition of forced response of acoustic pressure oscillations from limit-cycle to period-2 oscillations for increasing A_f at fixed $f_f/f_{n0} = 0.79$ which is at the frequency of the preferred mode of the flame; i.e. $f_f = f_q$. At $A_f = 10$ mV, the forcing amplitude is too low to effect any noticeable change in the limit-cycle dynamics (figure 11ii). At $A_f = 30$ mV, the response shows quasiperiodic dynamics, as can be seen from the $\mathbb{T}^2$-torus in the phase space (figure 11*c*iii). For $A_f = 50$ and 70 mV, we observe that the amplitude of limit-cycle oscillations at f_{n1} undergoes quenching (figure 11*b*iv,v), while the dynamics transitions to pronounced period-2 oscillations (figure 11*c*iv,v).

We conjecture that the observed period-2 behaviour in p' when $f_f \approx 290$ Hz ($f_f/f_{n0} \approx 0.79$) is due to the forcing signal exciting the fifth harmonic of the glass duct. The fifth harmonic is related to the preferred mode of the flame through the linear relation $f_5 \approx 2f_q$ (figure 2*b*). As a result, the high amplitude of forcing in the frequency range $280 < f_f < 300$ Hz excites the fifth harmonic of the combustor, resulting in the period-2 behaviour. Similar period-2 behaviour in the acoustic response has been reported in a numerical study by Kashinath *et al.* (2018). They reported a period-doubling route to chaos with increasing amplitude of forcing at $f_f = f_{n0}$. In contrast, we observe period-2 oscillations at $f_f = f_q \neq f_{n0}$. Moreover, we did not observe the period-doubling route to chaos because a further increase in the amplitude of forcing led to a loss of flame stability and the flame undergoes blow-out.

4. Conclusion

In this paper, we study the mechanism through which open-loop control of thermoacoustic instability is attained in a laminar premixed combustor with the aid of synchronization theory. We achieve open-loop control by subjecting the system to external harmonic forcing. We consider the acoustic pressure and HRR fluctuations to be two different oscillators having a disparate response when they are subjected to external forcing.

We draw the following conclusions from our analysis:

(i) We find that the flame possesses a preferred mode whose frequency is disparate from the acoustic eigenfrequencies of the combustor. When the limit-cycle oscillations are forced at a frequency around the frequency of the preferred mode of the flame, there is an amplification in the response amplitude of the HRR oscillations. Concurrently, we observe a reduction of 90 % and 99 % in the r.m.s. value and spectral amplitude of the pressure oscillations relative to the unforced values, respectively. This decrease in amplitude of thermoacoustic oscillations is a result of asynchronous quenching. We hypothesized that asynchronous quenching is observed only below f_{n0} because the frequency of the preferred mode is lower than the frequency of limit-cycle oscillations. We further showed that increasing the amplitude of forcing widens the frequency range over which asynchronous quenching can be effected. In practical systems, the presence of such a large region of quenching would then allow for the effective design of controllers with the flexibility of operation at one of these frequencies.

(ii) We show that the synchronization characteristics of the acoustic and HRR responses differ from each other significantly. In particular, we find that HRR oscillations are synchronized to forcing for a broader frequency range than the acoustic pressure oscillations. We also show that the maximum decrease in the amplitude of limit-cycle oscillations is attained only when both the acoustic and HRR oscillations synchronize with forcing.

(iii) We show that forcing causes asynchronous quenching when the forcing frequency is near the frequency of the preferred mode of the flame either (a) by causing the limit-cycle oscillations to be phase-locked with forcing or (b) by changing the dynamics of the acoustic response alone to period-2 oscillations. In the former case, the coupling is established at nearly $\pi/2$ rad out-of-phase, while in the latter case, there is phase drifting between acoustic and HRR oscillations due to differences in their dynamics. In either case, the time-averaged acoustic power production becomes very low, leading to the quenching of acoustic pressure oscillations.

(iv) We also provide the experimental evidence of period-2 behaviour in acoustic pressure fluctuations attained during the asynchronous quenching of limit-cycle oscillations. The fifth acoustic mode of the duct is related to the preferred mode of the flame through the relationship $f_5 \approx 2f_q$. So, forcing near f_q triggers the fifth harmonic (f_5) of the duct and leads to the period-2 oscillations. In this state, dynamics of acoustic pressure oscillations shows period-2 characteristics, while HRR oscillations retain period-1 limit-cycle oscillations.

As a final remark, we note that it may be possible to decouple the acoustic and the HRR response of a real-time combustor by introducing a forcing mechanism capable of perturbing the flame over a range of narrowband frequencies. The choice of forcing frequency depends on the parametric region for which we observe quenching of limit-cycle oscillations. A possible forcing mechanism, other than actuators, could

be a strategically placed delta wing or bluff body capable of generating vortices at a particular frequency upstream of the principal flame holder, thus affecting the flame directly. However, the applicability of such an open-loop control in turbulent combustors and practical gas turbine systems through such targeted forcing remains to be explored.

Acknowledgements

A.R. gratefully acknowledges the Ministry of Human Resource Development (MHRD) for funding a PhD through Half-Time Research Assistantship (HTRA). S.M. acknowledges the Institute Post-Doctoral Fellowship, IIT Madras. The role of Mr S. Thilagaraj in fabricating different components of the experimental set-up is gratefully acknowledged. This work was supported by Office of Naval Research Global (contract monitor: Dr R. Kolar) grant no. N62909-18-1-2061. We are indebted to an anonymous reviewer who reviewed our work thoroughly and gave numerous valuable suggestions.

Appendix A. Phase-space reconstruction

We construct the phase space using the delay embedding theorem proposed by Takens (1981). The theorem lays down the conditions under which the phase space can be reconstructed from a sequence of scalar measurements of the system dynamics. The reconstructed manifold has a one-to-one mapping to the original manifold, thus preserving the topology of the manifold and its dynamical invariants such as Lyapunov's exponent, correlation dimension, etc.

Here, we unfold the original attractor into an m-dimensional Euclidean delay vector space, capturing different segments of history of a given variable X:

$$\boldsymbol{\xi}(t) = [X(t), X(t+\tau), X(t+2\tau), \ldots, X(t+(m-1)\tau)], \quad \boldsymbol{\xi} \in \mathbb{R}^m. \tag{A 1}$$

Here, X represents the measured variables $\{p', \dot{q}'\}$.

For faithfully reconstructing the phase space, determination of the optimum time delay, τ, and minimum embedding dimension, m, is crucial. If τ is too low, the vectors would be very strongly correlated, while if it is too large, the vectors would be weakly correlated, prone to random noise and numerical inaccuracies. Optimum time lag will result in m mutually independent vectors over which the attractor can be unfolded to the maximum possible extent.

The optimum time lag was calculated using average mutual information (Fraser & Swinney 1986). The average mutual information indicates the average information about $X(t+\tau)$ that can be predicted from the original vector $X(t)$, and is calculated as

$$I(\tau) = \sum_{i=1}^{n} P[X(t_i) \cap X(t_i+\tau)] \log_2 \frac{P[X(t_i) \cap X(t_i+\tau)]}{P[X(t_i)]P[X(t_i+\tau)]}, \tag{A 2}$$

where n is the number of samples and P is the probability that $X(t)$ has a value of $X(t_i)$, and $P[X(t_i) \cap X(t_i+\tau)]$ indicates the joint probability. The time at which $I(\tau)$ attains its first local minima is considered to be the optimum time delay. For the unforced limit-cycle oscillations, the variations of the average mutual information as a function of the non-dimensional time delay (τf_{n0}) for p' and $\dot{q}'$ are plotted in figures 12(*a*) and 12(*b*), respectively.

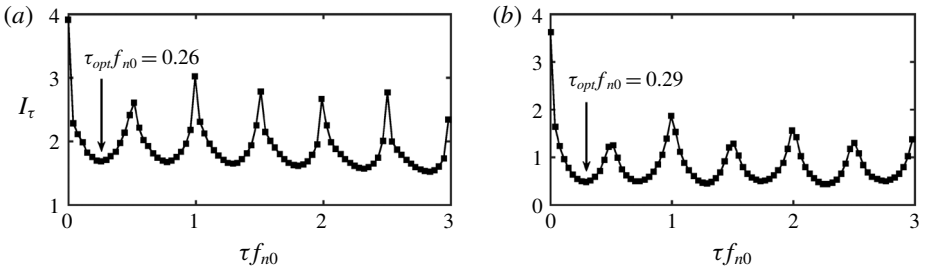

FIGURE 12. The average mutual information as a function of the non-dimensional time lag for (*a*) p' and (*b*) $\dot{q}'$ signals during unforced limit-cycle oscillations. The corresponding value of optimum time lag is indicated at the location of the first minima of the average mutual information.

The embedding dimension, m, is determined through Cao's method (Cao 1997). This is an optimized version of the false nearest-neighbour method. A false neighbour to a point in the phase space is that which moves away from its nearest neighbour with an increase in the embedding dimension. In Cao's method, the number of false neighbours that each point has in the phase space is tracked as the embedding dimension is increased. Given the optimum delay, we can then construct the measure $a(i, m)$ as

$$a(i, m) = \frac{\|X_i(m+1) - X_{n(i,m)}(m+1)\|}{\|X_i(m) - X_{n(i,m)}(m)\|}, \tag{A 3}$$

where $i = 1, 2, \ldots, (N - m\tau)$ and $n(i, m)$ is the index of the point nearest to point X_i in the phase space. Here $\|\cdot\|$ is the Euclidean norm between two points. We can average over the false neighbours to obtain a measure only dependent on the embedding dimension and the optimum time lag as

$$E(m) = \frac{1}{N - m\tau_{opt}} \sum_{i=1}^{N-m\tau_{opt}} a(i, m). \tag{A 4}$$

The increase in the measure with an increase in the embedding dimension can be determined by defining $E_1(m)$ as

$$E_1(m) = \frac{E(m+1)}{E(m)}. \tag{A 5}$$

The minimum embedding dimension required for the input signal $X(t)$ is determined as the dimension above which $E_1(m)$ saturates. Since all acoustic and HRR signals that we acquire are deterministic with well-defined periodicity during the state of thermoacoustic instability, the minimum embedding dimension calculated in this manner suffices for our objective (Nair 2014). The measure E_1 as a function of the embedding dimension has been plotted in figure 13 for p' and $\dot{q}'$ exhibiting limit-cycle oscillations and no external forcing. For unforced cases, $m = 5$ is enough to reconstruct the limit-cycle attractors; however, for cases where the dynamics shows a quasiperiodic behaviour in the presence of forcing, $m = 8$ is required. For visualizing

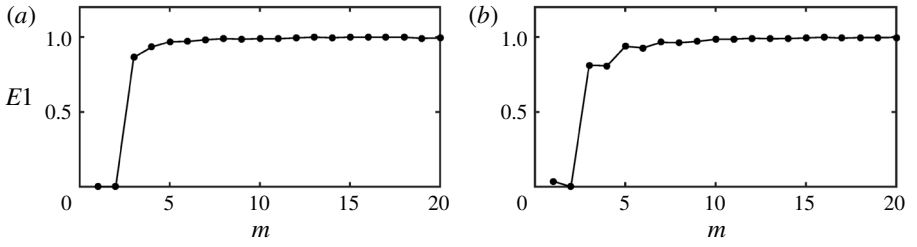

FIGURE 13. The variation of the measure E_1 as a function of the dimension (m) for (a) p' and (b) $\dot{q}'$ associated with unforced limit-cycle oscillations, determined from Cao's method.

the qualitative features of the attractor for all cases, we project the trajectories onto $m = 3$, as shown in figures 5(c) and 7(c).

REFERENCES

BALANOV, A., JANSON, N., POSTNOV, D. & SOSNOVTSEVA, O. 2008 *Synchronization: From Simple to Complex*. Springer Science & Business Media.

BALUSAMY, S., LI, L. K. B., HAN, Z. & HOCHGREB, S. 2017 Extracting flame describing functions in the presence of self-excited thermoacoustic oscillations. *Proc. Combust. Inst.* **36** (3), 3851–3861.

BALUSAMY, S., LI, L. K. B., HAN, Z., JUNIPER, M. P. & HOCHGREB, S. 2015 Nonlinear dynamics of a self-excited thermoacoustic system subjected to acoustic forcing. *Proc. Combust. Inst.* **35** (3), 3229–3236.

BELLOWS, B. D., HREIZ, A. & LIEUWEN, T. C. 2008 Nonlinear interactions between forced and self-excited acoustic oscillations in premixed combustor. *J. Propul. Power* **24** (3), 628–630.

CAO, L. 1997 Practical method for determining the minimum embedding dimension of a scalar time series. *Physica* D **110** (1–2), 43–50.

DOCQUIER, N. & CANDEL, S. M. 2002 Combustion control and sensors: a review. *Prog. Energy Combust. Sci.* **28** (2), 107–150.

DOWLING, A. P., HOOPER, N., LANGHORNE, P. J. & BLOXSIDGE, G. J. 1988 Active control of reheat buzz. *AIAA J.* **26** (7), 783–790.

DOWLING, A. P. & MORGANS, A. S. 2005 Feedback control of combustion oscillations. *Annu. Rev. Fluid Mech.* **37**, 151–182.

FJELD, M. 1974 Relaxed controls in asynchronous quenching and dynamical optimization. *Chem. Engng Sci.* **29** (4), 921–933.

FRASER, A. M. & SWINNEY, H. L. 1986 Independent coordinates for strange attractors from mutual information. *Phys. Rev.* A **33** (2), 1134–1140.

GABOR, D. 1946 Theory of communication. Part 1. The analysis of information. *J. Inst. Electrical Engrs-Part III: Radio Commun. Engng* **93** (26), 429–441.

GODAVARTHI, V., PAWAR, S. A., UNNI, V. R., SUJITH, R. I., MARWAN, N. & KURTHS, J. 2018 Coupled interaction between unsteady flame dynamics and acoustic field in a turbulent combustor. *Chaos* **28** (11), 113111.

GUAN, Y., GUPTA, V., KASHINATH, K. & LI, L. K. B. 2019*a* Open-loop control of periodic thermoacoustic oscillations: experiments and low-order modelling in a synchronization framework. *Proc. Combust. Inst.* **37** (4), 5315–5323.

GUAN, Y., HE, W., MURUGESAN, M., LI, Q., LIU, P. & LI, L. K. B. 2019*b* Control of self-excited thermoacoustic oscillations using transient forcing, hysteresis and mode switching. *Combust. Flame* **202**, 262–275.

HUERRE, P. & MONKEWITZ, P. A. 1990 Local and global instabilities in spatially developing flows. *Annu. Rev. Fluid Mech.* **22** (1), 473–537.

JUNIPER, M. P., LI, L. K. B. & NICHOLS, J. W. 2009 Forcing of self-excited round jet diffusion flames. *Proc. Combust. Inst.* **32** (1), 1191–1198.

JUNIPER, M. P. & SUJITH, R. I. 2018 Sensitivity and nonlinearity of thermoacoustic oscillations. *Annu. Rev. Fluid Mech.* **50**, 661–689.

KABIRAJ, L., SAURABH, A., WAHI, P. & SUJITH, R. I. 2012*a* Route to chaos for combustion instability in ducted laminar premixed flames. *Chaos* **22** (2), 023129.

KABIRAJ, L., SUJITH, R. I. & WAHI, P. 2012*b* Bifurcations of self-excited ducted laminar premixed flames. *Trans. ASME J. Engng Gas Turbines Power* **134** (3), 031502.

KASHINATH, K., LI, L. K. B. & JUNIPER, M. P. 2018 Forced synchronization of periodic and aperiodic thermoacoustic oscillations: lock-in, bifurcations and open-loop control. *J. Fluid Mech.* **838**, 690–714.

KEEN, B. E. & FLETCHER, W. H. W. 1970 Suppression of a plasma instability by the method of 'asynchronous quenching'. *Phys. Rev. Lett.* **24** (4), 130–134.

KINSLER, L. E., FREY, A. R., COPPENS, A. B. & SANDERS, J. V. (Eds) 1999 *Fundamentals of Acoustics*, 4th edn., p. 560. Wiley-VCH.

KUZNETSOV, Y. A. 2013 *Elements of Applied Bifurcation Theory*, vol. 112. Springer Science & Business Media.

LACHAUX, J.-P., RODRIGUEZ, E., MARTINERIE, J. & VARELA, F. J. 1999 Measuring phase synchrony in brain signals. *Human Brain Mapping* **8** (4), 194–208.

LANG, W., POINSOT, T. & CANDEL, S. 1987 Active control of combustion instability. *Combust. Flame* **70** (3), 281–289.

LI, L. K. B. & JUNIPER, M. P. 2013*a* Lock-in and quasiperiodicity in a forced hydrodynamically self-excited jet. *J. Fluid Mech.* **726**, 624–655.

LI, L. K. B. & JUNIPER, M. P. 2013*b* Lock-in and quasiperiodicity in hydrodynamically self-excited flames: experiments and modelling. *Proc. Combust. Inst.* **34** (1), 947–954.

LI, L. K. B. & JUNIPER, M. P. 2013*c* Phase trapping and slipping in a forced hydrodynamically self-excited jet. *J. Fluid Mech.* **735**, R5.

LIEUWEN, T. C. & NEUMEIER, Y. 2002 Nonlinear pressure-heat release transfer function measurements in a premixed combustor. *Proc. Combust. Inst.* **29** (1), 99–105.

LIEUWEN, T. C. & YANG, V. 2005 *Combustion Instabilities in Gas Turbine Engines (Operational Experience, Fundamental Mechanisms and Modeling)*. American Institute of Aeronautics and Astronautics.

LUBARSKY, E., SHCHERBIK, D. & ZINN, B. T. 2003 Active control of instabilities in high-pressure combustor by non-coherent oscillatory fuel injection. *AIAA Paper* 2003-4519.

MATSUI, Y. 1981 An experimental study on pyro-acoustic amplification of premixed laminar flames. *Combust. Flame* **43**, 199–209.

MONDAL, S., PAWAR, S. A. & SUJITH, R. I. 2017 Synchronous behaviour of two interacting oscillatory systems undergoing quasiperiodic route to chaos. *Chaos* **27** (10), 103119.

MONDAL, S., PAWAR, S. A. & SUJITH, R. I. 2019 Forced synchronization and asynchronous quenching of periodic oscillations in a thermoacoustic system. *J. Fluid Mech.* **864**, 73–96.

NAIR, V. 2014 Role of intermittency in the onset of combustion instability. PhD thesis, IIT Madras.

NAYFEH, A. H. & BALACHANDRAN, B. 2008 *Applied Nonlinear Dynamics: Analytical, Computational, and Experimental Methods*. John Wiley & Sons.

NOIRAY, N., DUROX, D., SCHULLER, T. & CANDEL, S. 2007 Passive control of combustion instabilities involving premixed flames anchored on perforated plates. *Proc. Combust. Inst.* **31** (1), 1283–1290.

NOIRAY, N., DUROX, D., SCHULLER, T. & CANDEL, S. 2008 A unified framework for nonlinear combustion instability analysis based on the flame describing function. *J. Fluid Mech.* **615**, 139–167.

OEFELEIN, J. C. & YANG, V. 1993 Comprehensive review of liquid-propellant combustion instabilities in F-1 engines. *J. Propul. Power* **9** (5), 657–677.

OHE, K. & TAKEDA, S. 1974 Asynchronous quenching and resonance excitation of ionization waves in positive columns. *Beiträge aus der Plasmaphysik* **14** (2), 55–65.

ORCHINI, A. & JUNIPER, M. P. 2016 Flame double input describing function analysis. *Combust. Flame* **171**, 87–102.

PAWAR, S. A., SUJITH, R. I., EMERSON, B. & LIEUWEN, T. C. 2018 Characterization of forced response of density stratified reacting wake. *Chaos* **28** (2), 023108.

PIKOVSKY, A. & MAISTRENKO, Y. L. 2012 *Synchronization: Theory and Application*. Springer Science & Business Media.

POINSOT, T. & VEYNANTE, D. 2005 *Theoretical and Numerical Combustion*. RT Edwards, Inc.

RAYLEIGH, J. W. S. 1878 The explanation of certain acoustical phenomena. *Nature* **18** (455), 319–321.

RICHARDS, G. A., STRAUB, D. L. & ROBEY, E. H. 2003 Passive control of combustion dynamics in stationary gas turbines. *J. Propul. Power* **19** (5), 795–810.

SHCHERBIK, D., LUBARSKY, E., NEUMEIER, Y., ZINN, B. T., MCMANUS, K., FRIC, T. F. & SRINIVASAN, S. 2003 Suppression of instabilities in gaseous fuel high-pressure combustor using non-coherent oscillatory fuel injection. In *ASME Paper No. GT2003-38103*.

SUJITH, R. I., WALDHERR, G. A. & ZINN, B. T. 1995 An exact solution for one-dimensional acoustic fields in ducts with an axial temperature gradient. *J. Sound Vib.* **184** (3), 389–402.

TAKENS, F. 1981 Detecting strange attractors in turbulence. In *Dynamical Systems and Turbulence, Warwick 1980*, pp. 366–381. Springer.

ZHAO, D., LU, Z., ZHAO, H., LI, X. Y., WANG, B. & LIU, P. 2018 A review of active control approaches in stabilizing combustion systems in aerospace industry. *Prog. Aerosp. Sci* **97** (2), 1–28.

ZHAO, D. & MORGANS, A. S. 2009 Tuned passive control of combustion instabilities using multiple Helmholtz resonators. *J. Sound Vib.* **320** (4), 744–757.